EUR 4909 e

COMMISSION OF THE EUROPEAN COMMUNITIES

POST-IRRADIATION ANALYSIS OF TRINO VERCELLESE REACTOR FUEL ELEMENTS

by

A.M. BRESESTI, M. BRESESTI, S. FACCHETTI, F. MANNONE, P. BARBERO, C. CERUTTI, F. MARELL, A. PEIL, R. PIETRA
(Chemistry Division)

R. KLERSY, A. SCHÜRENKÄMPER, A. FRIGO, E. GHEZZI, J.P. MEERSCHMAN, A. POLLICINI, K.H. SCHRADER
(Materials Division)

J. BITEAU (Essor Division)

A. CRICCHIO, L. KOCH
(Transuranium Institute, Karlsruhe)

1972

Joint Nuclear Research Centre
Ispra Establishment - Italy

and

Joint Nuclear Research Centre
Karlsruhe Establishment - Germany

ABSTRACT

Under the joint EURATOM-ENEL research program for the development of water reactor technology, post-irradiation analyses were carried out on three fuel assemblies irradiated at 8,000 to 14,000 MWd/t (U) in the TRINO VERCELLESE pressurized water reactor.

Visual and photographic examinations of selected fuel rods and metallography of fuel and canning materials showed a very good irradiation behaviour of the fuel elements.

The main objective of the program was the determination of burnup and isotopic composition of selected fuel samples in order to evaluate the accuracy of the calculation methods developed by FIAT NUCLEARE. Radioactive fission products have been measured by gamma spectrometry. The fission product Nd-148 and the uranium and plutonium nuclides have been determined by mass spectrometry combined with isotopic dilution techniques.

The experimental data obtained for burn-up and for the concentrations of uranium and plutonium nuclides have been compared with theoretical predictions obtained by means of computer codes.

KEYWORDS

SELNI REACTOR
FUEL ELEMENT CLUSTERS
IRRADIATION
PHOTOGRAFIC FILM DOSEMETERS
PHOTOGRAFIC FILMS
METALLOGRAPHY
FUEL CANS
BURNUP
ISOTOPE RATIO
FISSION PRODUCTS
GAMMA SPECTROSCOPY
PLUTONIUM
GAMMA FUEL SCANNING
URANIUM
ALPHA SPECTROSCOPY
MECHANICAL DECLADDING
COMPUTER CALCULATIONS
NEODYMIUM 148
MASS SPECTROSCOPY

TABLE OF CONTENTS

LIST OF TABLES

LIST OF FIGURES

1. INTRODUCTION.

In the framework of the EURATOM-ENEL research contract No. 071-66-6 TEEI-RD, post-irradiation analyses on the spent fuel of the Trino Vercellese reactor core one were performed at the Ispra and Karlsruhe Establishments of the EURATOM Joint Research Center.

The main objective of the post-irradiation examination program was the measurement of the burnup and the isotopic composition of selected fuel samples in order to evaluate the accuracy of the calculation methods developed by FIAT NUCLEARE in the framework of the EURATOM-FIAT research contract No. 098-66-6 TEEI-RD.

The other objective of the program was the metallographic analysis of the UO_2 fuel and of the stainless steel cladding.

The fuel assemblies selected for the analyses were dismantled at Ispra, in the pool of the ESSOR reactor. The removed fuel rods were subjected to visual examination. Gamma-scanning measurements were then made on the fuel rods in order to determine the axial distribution of the radioactive fission products, and consequently of the burnup.

Fuel and cladding samples were cut from the rods in selected positions for radiochemical and metallographic analyses.

The fuel samples for the radiochemical analyses were dissolved and aliquots of the solutions were subjected to radiochemical processes and to gamma, mass and alpha spectrometry determinations.

Gamma spectrometry was used mainly to determine the Cs-137 activity, from which the burn-up was derived; mass spectrometry, combined in some cases with isotope dilution techniques, was used to determine the concentrations and isotopic compositions of the heavy isotopes uranium, plutonium and americium, of Nd-148 and of the krypton and xenon fission gases; alpha spectrometry was used to determine the activities of some nuclides of plutonium, americium and curium.

The concentrations of the heavy isotopes and Nd-148 were then utilised for separate evaluations of the burnup.

The experimental values of burnup and uranium and plutonium isotopic contents were extensively compared with the theoretical prediction performed by FIAT NUCLEARE.

2. FUEL CHARACTERISTICS AND SELECTION OF FUEL SAMPLES.

2.1. Description of the reactor core and the fuel assemblies.

The Trino Vercellese Nuclear Power Plant, operated by Ente Nazionale per l'Energia Elettrica (ENEL), is equipped with a pressurized water reactor rated at 825 MW(th). Westinghouse Electric Corp. is the designer and manufacturer of the nuclear steam generating plant, fuel included.

The reactor was first brought to criticality on June 21, 1964. During the first cycle of power operation (October 23, 1964 - April 28, 1967) the fuel reached an average burnup level of 11,590 MWd/t(U).

The reactor core for cycle 1 was composed of 120 square fuel assemblies, divided into three radial zones of 40 assemblies each (initial enrichments 2.72, 3.13, 3.90%) and 52 cruciform assemblies (initial enrichment 2.72%). Of the 52 cruciform assemblies 28 are connected as "fuel bearing followers" to 28 cruciform control rods (absorbing material Ag - In - Cd). A cross section showing a quarter of the core is shown in Fig. 1.
Ten control rods act as a control group slightly inserted in the core during power operation; the remaining 18 rods act as shut-down rods and are fully withdrawn at power. The total initial weight of U in the core is 39.9 metric tons. The core is operated with chemical shim (boric acid dissolved in the coolant).

The core thermo-hydraulic characteristics are presented in Table 1.

A square fuel assembly consists of a 15 x 15 array of fuel rods. Portions of the peripheral rows of fuel rods are omitted to provide slots for the passage of the control rod blades. The central rod is also omitted to provide space for an in-core instrumentation thimble. The number of fuel rods for assembly is therefore 208. The fuel rods are kept in place by ten spacer grids welded to the perforated steel can which surrounds the fuel bundle.

Table 1 : Core thermo-hydraulic characteristics.

Power output	825 MW(th)
Coolant pressure	140 kg/cm^2
Coolant effective flow rate	16,000 t/h
Coolant inlet temperature	266.5°C
Coolant average temperature	282°C
Coolant outlet temperature	297.5°C
Core average power density	64.4 kW/l(21kW/kgU)
Max. design linear power density	12.4 kW/ft
Max. rod surface temperature	340°C

The cruciform fuel assemblies, of which 24 are permanently inserted in the core and 28 are attached to the 28 control rods, contain 26 fuel rods each. The control rods contain 32 absorber rods containing Ag, In, Cd in the ratio 80 : 15 : 5. The cladding material for the fuel and the absorber is stainless steel.

The main data relative to the fuel assembly and the control rod are presented in Table 2.

2.2. Irradiation history.

The post-irradiation analyses were performed on fuel irradiated during the first cycle of reactor operation (Oct. 23, 64 - Apr. 28, 67). Core average burnup at the end of the cycle was 11,590 MWd/t(U).

During the cycle two extended shut downs took place : the first for installation of a second TG unit, which allowed a power increase from 615 to 825 MW(th) and the second for maintenance and inspection of the TG unit No. 1. As a result the cycle may be considered divided into three periods summarized in Table 3.

Table 2 : Core mechanical data. (*)

CORE	
Equivalent diameter	249.9 cm
Active height	264.9 cm
Number of square fuel assemblies	120
Number of cruciform fuel assemblies	52
Number of regions	3
Initial enrichments (square assemblies)	2.72-3.13-3.90%
Initial enrichment (cruciform assemblies)	2.72%
Number of control rods	28
UO_2 in square fuel assemblies	42,321 kg
UO_2 in cruciform fuel assemblies	2,313 kg
Total UO_2 weight	44,634 kg
Total U weight	39,873 kg
SQUARE FUEL ASSEMBLY	
Rod array	15 x 15
Number of fuel rods	208
Side of square cross section	20.00 cm
Total length	320.88 cm
UO_2 weight	353.81 kg
FUEL PELLET	
UO_2 density	96.5 % T.D.
Diameter	0.890 cm
Length	1.53 cm
Dishing depth	0.33 mm
Number of pellets per rod (approx.)	173
Length of pellet stack in fuel rod	264.1 cm
Clad-pellet clearance	0.114 mm

(*) Nominal data, cold condition (cont.)

Table 2 (continuation)

FUEL CLAD	
Inside diameter	0.902 cm
Wall thickness	0.383 mm
Material	SS AISI 304
CRUCIFORM FUEL ASSEMBLY	
Number of fuel rods	26
Fuel length	240.3 cm
Rod outer diameter	1.092 cm
UO_2 weight	44.00 kg
CONTROL ROD	
Absorbing material	5% Cd-15% In-80% Ag
Cladding material	Type 304 SS
Number of absorber rods	32
Absorber length	269.2 cm
Absorber rod diameter	1.001 cm
Clad outer diameter	1.095 cm
Clad thickness	0.432 mm

Table 3 : Summary of cyle 1 operation.

Period	I	II	III
Date	23.10.64–5.6.65	31.8.65–20.5.66	11.7.66–28.4.67
Max.power level (MWth)	615	825	825
Coolant avg.temp. (°C)	282	278	278
Control group insertion	30%	4%	4%
Approx. boron concentration (ppm)	1300 ÷ 1050	1150 ÷ 650	650 ÷ 0
Core burnup (MWd/t(U))	2260	4085	5245

At the end of the cycle (with practically no boron in the coolant) a stretch-out operation was performed in two steps : first, rods were completely withdrawn and the full power level was maintained for 11 days by letting the average coolant temperature drop from 278°C to 274°C; finally the TG unit No.1 was shut down and the reactor power level was cut down to 300 MW(th) allowing two more weeks of operation.
The load diagram during the cycle is shown in Fig. 2.

2.3. Selection of fuel assemblies, rods and samples.

At the end of the first cycle, in addition to the 40 assemblies of the inner core region (enrichment 2.719 w/o), some assemblies of the intermediate and outer region (enrichment 3.130 and 3.897%) were also discharged from the reactor for reprocessing. Thus assemblies of the three enrichments were available for post-irradiation examinations. Therefore three fuel assemblies were selected, one for each initial enrichment.

The criteria for selection of assemblies, rods and samples have been the following :

- wide range of initial enrichment (2.719 ÷ 3.897 w/o)
- wide range of burnup values (8000 ÷ 14000 MWd/t(U) for the average of whole assemblies; 3000 ÷ 18000 MWd/t(U) for the single samples).
- different assembly location within the core (center, intermediate, periphery; near and away from control rods, etc.)
- different rod location within the assemblies (corner rods, rods near the central water hole provided for in-core instrumentation thimble, rods from normal positions) corresponding to different neutron spectra (perturbed and asymptotic)
- different axial location of samples along the rods in order to obtain axial profiles of burn-up and isotopic composition and to investigate the effect of the axial temperature gradient.

The core map showing assemblies and rods selected is given in Fig. 1.

The identification of sampling positions along the height of the assemblies is shown in Fig. 3.

A total of 8 rods and 21 samples were selected. The rods and samples selected for examination are summarized in Table 4.

Table 4 : Selected fuel samples.

Assembly Location	Average burnup (MWd/t(U))	Initial Enrichment (w/o)	Rod Number (see Fig.1)	Axial Locations (see Fig.3)	Comments
G-7	12380	2.719	1	1-4-9	Asymptotic spectrum
			2	1-4-7-9	Intermediate spectrum (near water hole)
			3	1-7-9	Perturbed spectrum(corner rod)
H-10	14170	3.130	4	1-4-7-9	Asymptotic spectrum
			5	4-7-9	Intermediate spectrum (near water hole)
			6	7	Perturbed spectrum(corner rod)
L-7	8660	3.897	7	7	Asymptotic spectrum
			8	1-7	Perturbed spectrum (core edge rod)

3. DISMANTLING OF THE FUEL ASSEMBLIES AND VISUAL EXAMINATION OF THE FUEL RODS.

The dismantling of the fuel assemblies and the recuperation of the selected fuel rods have been done in the water pool of the ESSOR reactor. The operation was performed by means of a special device designed by ENEL [1] and installed in the second tank of the pool (see Fig. 4). It consists of a tubular welded frame levelled on the bottom of the tank by four adjustable and stable feet. This frame supports a tilting basket containing the fuel assembly during cutting operations and allowing the basket to rotate after the fuel rod extraction, and a cutting device composed of a miller tool actuated by a pneumatic motor. The tilting basket is a long, square cross-section box, with flanged ends, on which the upper and lower special covers were mounted. It keeps the fuel assembly exactly in position with reference to the frame and hence to the cutting device. It may, after the cutting of the upper part of the cans, be substituted by a transportation cover; after rotation it presents a standard lifting end for manipulation and storage. The pneumatic motor is fixed on a support mounted on a slide movable on two cylindrical guides in a direction parallel to the face to be cut. The support can be regulated in a direction perpendicular to the movement of the slide to follow the shape of the cans with the cutting tool. All of the movements were actuated by long rods and a tubular spanner from the pool plateform. A chip suction water-ejector system actuated by a centrifugal pump with suitable filters to retain the radioactive chip was installed in the pool; the suction device was fixed on the miller support.

Operating procedures.

After the shipping cask containing the fuel assemblies was opened into the pool, the three fuel assemblies were drawn out by means of the lifting tool and stored in a storage rack. Each of the three assemblies was grabbed by the lifting tool already fitted with the "upper-cover" and transferred into the tilting basket. The upper cover is shaped as a stirrup in order to allow the cutting tool to enter from two opposite sides. It keeps the fuel assembly centered inside the basket to prevent vibrations during cutting operation.
The cutting device was then slid into position and actuated. The travel of the miller was manually actuated at a speed of three revolutions per minute, corresponding to 10 mm/minute. Once the first face had been cut, the tilting basket with its covers and the contained assembly was rotated by 180° around its vertical axis to present the opposite face to the cutting device. Before cutting the remaining two faces of the can, it was necessary to separate the lifting tool and the upper cover from the tilting basket and the fuel assembly, to rotate it by 90° and to fix it again in the new position. Then the tilting basket was rotated by 90° to present the third face to the cutting device. The cutting of the two remaining faces was performed in the same way as for the others.
After removal of the top end plate, the selected fuel rods were withdrawn and transported in the storage basket.
After the fuel assembly was closed with the perforated cover, the basket was closed by a temporary cover and inverted by rotating it on its trunnions. After removing the lower cover, the fuel assembly was grappled by means of the standard head, drawn out of the tilting basket and deposited directly in the shipping container.

Visual and photographic examination of the fuel rods.

Following their removal from the fuel element itself and their storage in the storage basket, the fuel rods were transferred in a specially designed transfer basket from the pool to the main examination cell of the ADECO.
Each rod was fixed on a support, which could slide in front of the lead windows of the cell. It was examined visually very carefully by means of a high magnification monocular periscope, a questar telescope and a special binocular. Then pictures were taken by means of a SINAR camera equipped with a 500 mm focal length lens. Four types of marks could be observed on the stainless steel fuel cans, which are illustrated by the following pictures :

a) Halos localized at the level where the flow regime of the coolant is modified by the springs of the grids (Fig. 5). These halos are brown coloured and lengthened with the coolant flow.

b) Black longitudinal scars which correspond to the spring positions (Fig. 6). These marks seem to have been produced by the spring during the assembly of the element and then filled by black deposits during the time in the reactor core.

c) Orange deposit spots. Fig. 7 shows an example of such a spot located between two grid levels. It has an almost perfectly circular shape : there is no attack of the clad in this position as the micrograph made at this point shows (Fig. 11).

d) Bright circumferential scars and points of fretting corrosion at the contact of the spring with the can. These defects are illustrated in Fig. 8 and 9. The micrograph of a cross section at the position (1) of Fig. 5 and 6 shows an attack of the surface of the rod (see Fig. 10).

In conclusion, the visual and optical examination of the fuel rods showed only a few small defects on the cans.

After examination, the fuel rods were cut in three parts using an abrasive disk cutting machine and then sent to the metallurgical hot laboratory.

4. METALLOGRAPHY OF FUEL AND SHEATH MATERIALS.

The scope of the metallographic analysis carried out in the hot lab was :

a) to clear up the importance of the macroscopic defects observed on the surface of the fuel rods (see Fig. 5 to 9)

b) to inspect the UO_2-fuel.

In the previous section, two types of circular defects have been observed. Corresponding samples have been cut off from the rods for metallographic examination. Fig. 10 shows the micrograph of a part of a cross-section, as polished and as etched, containing a defect shown in Fig. 9. One observes very clearly an attack on the surface of the rod. It may be caused in a mechanical way, for instance by friction of a spring. It does not seem indicative that the defect is due to a corrosion process. The examination of the defects shown in Fig. 7 revealed no attack of the surface at all. It must be concluded that they are only superficial spots. Fig. 11 shows a corresponding cross-section of the canning. No attack can be seen. The microstructure of the cladding material is homogeneous.

For the analysis of the fuel, rod No.8 with the lowest burnup and rod No. 4 with a high burnup have been chosen. In Fig. 12 and 13, one can see a cross section of these two rods, which show cracks typical for the fuel examined. Fig. 14 and 15 show micrographs of the fuel. In both cases, there is no significant difference between the microstructure observed in the fuel center and in the external zone of the fuel. Furthermore, there is no significant difference between the two fuel rods. Summarizing, one can say that the microscopic examination of the fuel led to the conclusion that, besides the cracking of the fuel, there was no particular modification

in the microstructure, which could be attributed to temperature or irradiation. This confirmed the result of temperature calculations on the fuel, which predicted a maximum temperature of about 1500°C. For this temperature no change of the microstructure of the fuel can be expected.

5. DETERMINATION OF BURNUP AND ISOTOPIC COMPOSITION.

5.1. Experimental analysis.

The selection of rods and pellets to be subjected to experimental determination of fission products and heavy isotopes has been presented in Section 2.

The program of analyses can be broadly divided into non-destructive measurements for the determination of radioactive fission products and destructive measurements for the determination of fission products and heavy isotopes.

Eight rods have been measured by means of non-destructive gamma spectrometry techniques in the laboratories of the Joint Research Center at Ispra.

In the selected positions, the eight fuel rods were cut and samples 10 mm thick were prepared for destructive analyses. The cutting positions were determined with an uncertainty of $\pm$ 3 mm. The fuel samples were dissolved with nitric acid in hot cells. Small aliquots of the fuel solutions, which can be handled without heavy shielding, are transferred to glove-boxes for radiochemical processes.
In the laboratories of the Joint Research Center at Karlsruhe the fission gases are collected during the fuel sample dissolution.

The analyses were performed at Ispra (18 samples) and Karlsruhe (3 samples + 5 for cross check).
At Ispra radioactive fission products have been determined by means of gamma spectrometry; Nd-148 and plutonium and uranium nuclides have been determined by isotopic dilution and mass spectrometry. In addition to these determinations, at Karlsruhe the isotopic compositions of the Kr and Xe fission gases and of americium have been measured by means

of mass spectrometry and the concentrations of some plutonium, americium and curium isotopes have been determined by alpha spectrometry.

In the present report, the experimental procedures adopted at Ispra are presented in detail and only a short description is given of the experimental procedures adopted at Karlsruhe. These latter procedures are described in detail in reference [2].

A flow sheet of the experimental determinations is reported in Fig. 16.

5.1.1. Non destructive gamma spectrometry.

Gamma scanning measurements of fuel rods give information about the axial distribution of radioactive isotopes in the fuel. Total gamma activity measurements needing a very simple experimental equipment can be considered as an overall inspection of the fuel. The activity will be very roughly proportional to the burn-up of the fuel after a long cooling time. Cracking of the fuel or sintering between different fuel pellets may be indicated by the gross gamma scanning.

Using a Ge-Li crystal, the axial distribution of the gamma activity of single isotopes can be determined. If, during reactor operation, no significant migration of fission products occurred, the measured activities should be proportional to the concentration of the corresponding isotopes. In this case, all conclusions which can be drawn from a destructive gamma spectrometry can also be made from the non-destructive gamma scanning measurements. In particular, if the burnup of the fuel can be inferred from Cs-137, the gamma scanning allows a burnup determination.

5.1.1.1. Gamma scanning equipment.

The apparatus used consists of a mechanical part installed inside a hot cell (Fig. 17), a collimator system mounted in the concrete wall of the cell and the equipment for gamma-ray analysis which is installed outside the hot cell. An electronic control unit allows measurements to be run automatically following a preselected program for the displacement of the fuel rod and counting time. During counting the rod was rotated, but its vertical axis was fixed. The collimator had an aperture of 0.5 mm height and 20 mm width.
To analyse the gamma-rays, a NaI crystal and a Ge-Li drifted detector have been used with a 400 channel analyser.

5.1.1.2. Gross gamma scanning.

The maximum length of a fuel rod which could be mounted on the mechanical scanning system was 130 cm. Therefore, the fuel rods of 3 m length had to be cut in three parts, which have been analysed separately.

The distribution of the total gamma activity in the energy range from 50 KeV to 2500 KeV was measured using the NaI crystal. These activities were determined in steps of 0.5 mm in an axial direction. Due to the rotation of the rod, mean values of the different sections were obtained. Fig. 18 shows a typical result of the measured activity distribution of a part of a fuel rod. One can see a number of equidistant well-pronounced minima. They are due to the interfaces between two fuel pellets 14.8 mm long. The scattering of the activity between two of these minima has to be considered as a statistical one. The less pronounced decrease of activity extended over a rather large region is due to the presence of structure material in the reactor core, in this case grid of the fuel element.

Results.

In Fig. 19 to 26 the results for the eight fuel rods examined are shown. The three parts of the rods, measured separately, are reassembled in the figures, with the exception of the rod number 3, which has been cut in two parts.

Evidently, the decrease of the activity near the cutting sections is caused by the experimental arrangement and is not due to a local decrease of the concentration of fission products.

The points of the rods where gamma spectrometry has been carried out (1,2,4,7,8,9) (see also Fig. 3), are indicated as well as the location of fuel samples cut off for the isotopic analysis by mass spectrometry.

The following conclusions may be drawn from the results we have obtained (Fig. 19-26) ;

- All the fuel rods show well pronounced minima of activity due to the interface of different fuel pellets. This indicates that no metallurgical interaction between different pellets occurred during irradiation and confirms the metallographic examination of the fuel.

- All fuel rods show a decrease of activity near the grid positions (Fig. 19). This corresponds to a real decrease of the burnup due to the flux depression caused by the displacements of water by the grids.

- The fuel rods from the angular positions (No. 3 and 6) show flux depressions due to the mechanical structure of the fuel box (see Fig. 21 and 24).

Fig. 26 shows the influence of the formers of the fuel element on the burnup distribution of fuel rod number 8, (peripherical position of the external zone of the core). The displacement of water by these formers leads to a flux depression in their neighbourhood.

5.1.1.3. Measurements of fission product concentrations.

Gamma ray intensities of Cs-137, Cs-134 and Ru-106 have been determined using a Ge-Li crystal. The activity of Ce-Pr-144 has been measured using a NaI crystal. Fig. 27 shows a typical gamma spectrum obtained with the Ge-Li crystal. Measurements of the reproducibility of the areas of the peak led to a dispersion of 1.5% for the Cs-137, of 2.5% for the 796 KeV ray of the Cs-134 and to 3% for the 513 KeV ray of Ru-106. The gamma scanning measurements have been carried out over a long period. In this time the crystal changed its characteristics a little. Therefore, the precision of the areas measured, may be worse than indicated previously.

Results.

The experimental results obtained are listed in Table 5. Activities are expressed in counts per minute. All values are corrected for decay, the reference time is the end of reactor operation. All the measurements have been made using the same geometry with the same counting equipment.

Gross gamma scanning and metallographic examination indicated that there was no significant migration of fission products. Therefore, the observed activities should be proportional to the concentration of the corresponding isotopes. On 18 samples these concentrations have been determined in a destructive test. A statistical analysis has been carried out, to compare the values from the gamma scanning measurements with the values from the destructive tests.

For the four isotopes a regression equation

$$y = b\,x + c \qquad (1)$$

has been calculated, where

Table 5 : Gamma ray intensities (counts/min).

Fuel element	G-7			H-10			L-7		
Fuel rod	1	2	3	4	5	6	7	8	
Axial Pos.									
1	312.3	333.9	331.2	289.0	330.3	368.6	227.5	140.8	
2	469.6	474.8	499.2	479.5	508.0	495.1	302.6	196.6	Cs-137
4	552.7	566.4	605.8	554.6	627.6	630.1	453.9	259.1	662 KeV
7	543.8	581.5	620.8	574.6	693.6	636.0	479.1	288.5	
8	533.2	566.9	569.0	565.3	527.8	635.6	440.5	244.6	
9	430.2	410.5	432.8	461.5	472.2	519.6	339.8	202.3	
1	172.5	172.7	184.4	132.1	167.6	207.1	78.7	18.3	
2	352.3	409.3	406.3	356.6	427	502.7	163	52.3	Cs-134
4	486	532.9	541.5	533	593.5	617.1	276.4	75	
7	480.6	510	560.5	518	635	665.5	334	94	796 KeV
8	434.7	438.6	485.5	486.9	496	592	284.3	80.3	
9	290	257.2	310.5	347.3	337.6	447	174	46.1	
1	359.9	431.5	375	323	296.9	388.2	138	71.8	
2	579.5	690.8	632	541.8	601.5	725.7	217.6	65.6	
4	723.7	701	820	734	848	864.7	313	183.9	Ru-Rh-106
7	718.8	772.3	807.2	774.7	708	918.5	300.1	180.1	513 KeV
8	676.5	609	755.4	579.2	625.4	853.8	282.3	185.6	
9	501.3	408.6	531.9	531.3	490.3	648.2	223.8	162.6	
1	1200	1354	1300	1201	1485	1472	1051	717	
2	1708	1915	1878	1915	2181	2134	1335	967	
4	1920	2015	2093	2105	2323	2401	1817	1122	Ce-Pr-144
7	1889	2044	2227	2097.8	2304	2546	1848	1211	2180 KeV
8	1820	1955	2126	2032	2220	2458	1742	1046	(NaI-crystal)
9	1593	1512	1878	1715	1921	2097	1371	953	

x is the activity in counts/min from gamma scanning measurement ;

y is the concentration of the isotopes expressed in Curies per gram of initial uranium.

Results are given in Table 6.
In addition to the regression equation, the correlation of x versus y and the standard error of b is indicated. The equations can be used for the determination of fission product concentrations. To get information about the precision, the standard error of the estimated values (given by the equations of Table 6) for given x values has been calculated. This standard error depends on the value of x. It is a minimum for the mean values $\bar{x}$ of the 18 values used for the regression analysis. In Table 7 results are listed. One can see that the standard error in the range of experimental x-values is smaller than 1.7% for Cs-137, 4% for Cs-134, 1.7% for Ce-Pr 144 and 7.7% for Ru-Rh 106, if one excludes the extremely low values of the rod number 8.

The results of the destructive and non-destructive measurements of Cs-137 are in good agreement. Therefore, a direct comparison of the burnup determination with the Cs-137 activity measurements has been made. Taking the results of the burnup determination obtained by measuring the heavy elements and the Nd-148 concentration (Table 20) and the results of gamma scanning measurements, a regression analysis leads to the following relationship

$$y = 27{,}7x - 663 \qquad (2)$$

where x is the activity of Cs-137 in counts/min obtained from gamma scanning, and

y the burnup in MWd/t(U).

Table 6 : Calibration of gamma scanning measurements.

Isotope	Correlation Coefficient	Regression Equation	Standard error of Regression Coefficient S.E.(b)
Cs-137	0.992	$y = 0.865 \cdot 10^{-4} \quad x - 0.109 \cdot 10^{-2}$	$0.252 \cdot 10^{-5}$ (3.0%)
Cs-134	0.995	$y = 0.889 \cdot 10^{-4} \quad x - 0.641 \cdot 10^{-3}$	$0.213 \cdot 10^{-5}$ (2.5%)
Ce-Pr-144	0.990	$y = 0.313 \cdot 10^{-3} \quad x + 0.312 \cdot 10^{-1}$	$0.109 \cdot 10^{-4}$ (3 %)
Ru-Rh-106	0.951	$y = 0.294 \cdot 10^{-3} \quad x + 0.106 \cdot 10^{-1}$	$0.239 \cdot 10^{-4}$ (8.1%)

x : gamma activity in counts/min

y : fission product concentration in Curies/g initial uranium

$$S.E.(b) \quad \frac{\sigma}{\sqrt{\sum_{i=1}^{n}(x_i-\bar{x})^2}} \quad \text{with} \quad \sigma^2 = \frac{\sum_{i=1}^{n}(y_i-\bar{y})^2 - b^2\sum_{i=1}^{n}(x_i-\bar{x})^2}{n-2}$$

$\bar{x}$, $\bar{y}$: mean values of the experimental observations

Table 7 : Precision of estimated fission product concentrations using the calibration of Table 6.

Isotope	Mean values $\bar{x}$	Mean values $\bar{y}$	Standard error about the regression σ *		Standard error of the regression estim. in the range of the experimental data S.E.(y)
Cs-137	$0.457 \cdot 10^{3}$	$0.381 \cdot 10^{-1}$	$0.153 \cdot 10^{-2}$	4.1%	0.8 - 1.7 %
Cs-134	$0.351 \cdot 10^{3}$	$0.306 \cdot 10^{-1}$	$0.173 \cdot 10^{-2}$	5.6%	0.8 - 4.0 %
Ce-Pr-144	$0.173 \cdot 10^{4}$	$0.574 \cdot 10^{0}$	$0.216 \cdot 10^{-1}$	3.7%	1.2 - 1.7 %
Ru-Rh-106	$0.526 \cdot 10^{3}$	$0.165 \cdot 10^{0}$	$0.220 \cdot 10^{-1}$	13.3%	3.7 - 7.7 %

* see Table 6

$$S.E.(y) = \sigma \sqrt{\frac{1}{n} + \frac{(x_k - \bar{x})^2}{\sum_{i=1}^{n} (x_i - \bar{x})^2}}$$

The standard deviation of the regression coefficient is 0.623 or 2.3%. The correlation coefficient is 0.988. In the interval of the measured Cs-137 activities the calibration line gives the burnup values with a standard deviation between 0.7 and 2.0% for a fixed value of x (if one excludes the extreme low values of the rod number 8). That means that, in the case of the Trino Vercellese fuel elements, the measurement of Cs activity by non-destructive gamma scanning gives quite a good method for the burnup determination. The discussion of the burnup values has been dealt with in the chapter 5.3.2.

In Table 25 the experimental results obtained are compared with theoretical calculated values.

It may be mentioned that the linear relationship

$$y = 8.51\ x - 2722 \qquad (3)$$

has been found between the Ce-144 activity (counts/min) and the burnup in MWd/t(U). The standard deviation of the regression coefficient is 2.8%, the correlation coefficient 0.982.

5.1.2. Destructive gamma spectrometry.

The aim of these measurements is the evaluation of the burnup level by determining the specific activities of radioactive fission products in the fuel solutions. For this purpose, known aliquots of the diluted fuel solution were subjected to gamma spectrometry, with Ge(Li) and NaI(Tl) detectors connected through a preamplifier and an amplifier to a multichannel analyser. Two Ge(Li) detectors :

1) Ge(Li) coaxial type 20 cm^3 FWHM ~3.5 KeV at 1.33 MeV

2) Ge(Li) coaxial type 20 cm^3 FWHM ~2 KeV at 1.33 MeV

and one 3" x 3" NaI(Tl) detector were utilized for the measurements. Fig. 28 shows a gamma spectrum of fission products in the energy range 100-900 KeV obtained with the Ge(Li) detector No. 2. The isotopes and gamma lines selected for the measurements are reported in Table 8.

Table 8 : Nuclear data of the radioactive fission products.

ISOTOPE	ENERGY (KeV)	HALF-LIFE
Ce-144	134 and 2186	284 d
Ru-106	512	367 d
Cs-137	662	30.5 y
Cs-134	796 + 802	2.05 y

In the case of the isotope Ce-144, at the beginning of the measurements both the gamma photopeaks at 134 KeV -measured with Ge(Li) detector- and at 2186 KeV- measured with NaI(Tl) detector- were evaluated. The two independent measurements were in a very good agreement and so it was decided to evaluate only the gamma line at 134 KeV.

In the case of the isotope Cs-134 the gamma line at 605 KeV was not considered, in order to avoid interference from the fission product Sb-125 (E_γ = 601 + 607 KeV, h.l. = 2.7 y).

This interference was evaluated to be between about 7% (for low burnup level) and 3% (for high burnup level) at the date of measurements (June 1970).

For the determination of the burnup level, only the results of Cs-137 were utilized. The results of the measurements on the fission products Cs-134, Ce-144, Ru-106 were utilized for studies of isotope correlations in irradiated fuels which are of interest both for problems of fissile material management and for problems of nuclear safeguards. Some of the most interesting correlations obtained during the post-irradiation analyses are presented in Section 5.3.

Another possibility of the utilisation of the data on the fission products, is as a check of the accuracy of the neutron code calculations of the different types of fissions. In fact, the fission yields of Ce-144 and Ru-106 differ for fissions of U-235, U-238 and Pu-239. This check, which would require an additional processing of the neutron code output data, will possibly be made in the future within the framework of studies for nuclear safeguards.

Experimental.

For each fuel cross section solution, three weighed samples were taken and each sample was counted two or three times. The spectra obtained with the multichannel analyser were stored on a punched tape and elaborated by an IBM 360/65 computer with a computer code that gives the net area of the gamma photopeaks. The absolute activity of the selected isotopes was determined by comparison with reference sources of known activity and a similar geometry, supplied by the Radiochemical Center, Amersham.

The resulting counting rate (dis/sec) was corrected for decay since reactor shutdown (28 April 1967).

The uranium concentration in the solution was determined by isotopic dilution and mass spectrometry (see sections 5.1.3 and 5.1.4). In this way it was possible to calculate the specific activity of the selected isotopes expressed as dis/sec. g final uranium.

Results of the measurements and evaluation of the errors.

The specific activities of the fuel samples expressed as Ci/g final uranium at the reactor shutdown for the four selected isotopes are reported in Table 9. We notice that, for the calculation of the burnup values, it is necessary to correct for the small amount of uranium burnt during the irradiation.

An evaluation of the errors made in the determination of the specific activity of the four selected isotopes is reported in Table 10. In the last column the square root of the sum of each squared coefficient is reported.

Eight fuel cross-sections, five of which were adjacent to those analysed at Ispra, were analysed at the Karlsruhe Research Center. In these laboratories only the activity of the fission product Cs-137 was determined using the techniques described in Reference [2]. At Karlsruhe the uranium concentration in the fuel solution was determined by weighing the fuel sample and the fuel solution, so that the resulting data are the specific activities of Cs-137 expressed as Ci/g initial uranium.

All of the results obtained at Karlsruhe and the data obtained at Ispra for the five adjacent fuel cross-sections are reported in Table 11. The agreement between the data of the two laboratories is satisfactory with the exception of the samples G-7-3-1. For these samples a disagreement in the same sense was also observed for the measurements on uranium and plutonium. This fact supports the opinion that the

deviation does not derive from experimental errors, but from a real difference in the burnup of the two pellets. We wish to point out that all of the data reported in Table 9 and 11 are not corrected for the in-core decay.

Table 9 : Specific activity of the fuel samples at the reactor shutdown (Ci/g final uranium).

ASSEMBLY	ROD	AXIAL LOCATION	Ce-144	Ru-106	Cs-137	Cs-134
G-7	1	1	0.429	0.104	0.0256	0.0137
	1	4	0.669	0.222	0.0468	0.0427
	1	9	0.531	0.149	0.0345	0.0231
	2	1	0.456	0.112	0.0273	0.0158
	2	4	0.689	0.237	0.0486	0.0459
	3	1	0.485	0.122	0.0292	0.0165
	3	7	0.738	0.266	0.0537	0.0517
	3	9	0.610	0.177	0.0392	0.0287
H-10	4	1	0.438	0.0843	0.0243	0.0123
	4	4	0.734	0.217	0.0507	0.0477
	4	7	0.719	0.232	0.0514	0.0505
	4	9	0.567	0.158	0.0370	0.0276
	5	7	0.787	0.246	0.0568	0.0569
	5	9	0.642	0.172	0.0403	0.0305
	6	7	0.829	0.250	0.0590	0.0609
L-7	7	7	0.589	0.143	0.0397	0.0278
	8	1	0.238	0.0295	0.0120	0.00221
	8	7	0.386	0.0633	0.0242	0.00816

Table 10 : Errors in the determination of the specific activity of the fuel samples. (standard errors %).

Isotope	Dilution, weighing and counting of the fuel samples	Counting of the reference samples	Absolute activity of the reference samples (standard error + systematic error)	Uranium concentration of the fuel solutions	TOTAL
Ce-144	0.7	0.3	0.8	0.5	1.2
Ru-106	1	0.3	0.7	0.5	1.4
Cs-137	0.5	0.3	1.4	0.5	1.6
Cs-134	0.6	0.3	0.7	0.5	1.1

Table 11 : Comparison between Cs-137 determinations at Karlsruhe and Ispra. Specific activity of the fuel samples at the reactor shutdown (Ci/g initial uranium).

ASSEMBLY	ROD	AXIAL LOCATION	Cs-137	
			Karlsruhe	Ispra
G-7	1	4*	0.0453	0.0458
	1	9*	0.0339	0.0339
	2	7	0.0490	
	2	9	0.0362	
	3	1*	0.0250	0.0288
	3	7*	0.0514	0.0525
H-10	5	4	0.0531	
L-7	7	7*	0.0395	0.0390

* Pairs of adjacent fuel sections

5.1.3. Radiochemical processes.

The main purpose of the radiochemical processes was to obtain from the original fuel solution after an isotopic dilution step, a purified solution of uranium, or plutonium or neodymium, in a suitable condition to be analysed by mass spectrometry.

At Ispra, uranium and plutonium were individually purified from interfering materials by means of solvent extraction techniques. At Karlsruhe, an ion-exchange technique was utilised to reduce the ratio between uranium and plutonium and to purify both the elements in the same step.

Radiochemical processes have also been utilized at Karlsruhe for the purification of americium and fission gases to be measured by mass spectrometry.

A detailed description is only given for the radiochemical procedures utilized at Ispra. A description of the procedures utilized at Karlsruhe can be found in Reference [2].

Uranium purification procedure.

Known aliquots of the diluted sample solution (about 10 ug of uranium) and of the spike solution (about 5 ug of U-233) were mixed and evaporated to dryness in order to allow the conditioning of the solution to 1 M nitric acid.

After addition of 1 M nitric acid, the plutonium was reduced to the trivalent state by hydroxylamine hydrochloride and stabilized by ferrous sulphamate. The pH of the solution was then adjusted by dropwise addition of ammonium hydroxide, to the yellow form of metacresol-purple indicator corresponding to a pH of about 3.

After addition of aluminium nitrate, the solution (6.5 ml) was extracted (1 min) with 1.5 ml of 10% tributylphosphate (TBP) in iso-octane. The aqueous phase containing plutonium and fission products was discarded and the uranium was stripped (3 min) from the organic phase by 1 ml of an aqueous solution 0.9 N in sulphuric acid and 0.1 N in nitric acid.
After centrifugation the aqueous phase containing uranium was carefully separated from the TBP-phase and evaporated to dryness; 1 M nitric acid solution was then added to the residue in order to have a total uranium concentration of about 150 µg/g, suitable for mass spectrometry analyses.

For each dissolved fuel cross-section, three U-233 spiked and three unspiked samples was purified for subsequent mass spectrometry analyses.

Plutonium purification procedure.

Known aliquots of the diluted sample solution (about 1 µg of plutonium) and of the spike solution (about 0.25 µg of Pu-242) were mixed with concentrated nitric acid and carefully evaporated to dryness in order to insure the depolymerization of Pu and to allow the conditioning of the solution to 0.5 M nitric acid.

After addition of 0.5 M nitric acid, the plutonium was reduced to the trivalent state by hydroxylamine hydrochloride at 80°C for 10 min. and then oxidized to the tetravalent state by sodium nitrite. This redox treatment was made in order to have all the Pu in an extractable form and to promote its isotopic exchange.

After adjustment to 1 M nitric acid, the solution was extracted (10 min) with an equal volume of 0.5 M thenoyltrifluoroacetone(TTA) in xylene. The aqueous phase containing uranium and fission products was discarded and the organic phase containing plutonium was scrubbed (5 min) with an equal

volume of 1 M nitric acid in order to remove uranium traces. After separation from the aqueous phase, the plutonium was then stripped (5 min) from the organic phase with an equal volume of 8 M nitric acid.

After centrifugation the main part of the 8 M nitric acid containing plutonium was removed very carefully from the T.T.A.-phase.

In order to eliminate eventual traces of organic solvent which interfere with mass spectrometry measurements, the aqueous phase containing plutonium was evaporated twice to dryness after addition of small aliquots of concentrated perchloric acid. The residue was dissolved in 1 M nitric acid in order to have a total plutonium concentration of about 15 µg/g of solution, suitable for mass spectrometric analyses.

As in the case of uranium, for each dissolved fuel cross-section three Pu-242 spiked and three unspiked samples were purified for subsequent mass spectrometric analyses.

Neodymium purification procedure.

Known aliquots of the sample solution (1-2 µg of Nd-148, about 7 M in nitric acid) and of the spike solution (about 1 µg of Nd-150) were mixed with 40% HF in order to have a 6 M nitric and 6 M hydrofluoric acid solution.

The solution was loaded onto anhydrous manganese dioxide (AMD) column, 0.7 cm internal diameter and 3 cm long, in order to separate the rare earths from the main part of the most important gamma-ray emitters. The flow rate was 1 ml/minute. Uranium, plutonium and fission products (except the rare earths) were eluted with 6 M HF, and the rare earths subsequently eluted with 8 M HNO_3.

Another important gamma-emitter is Ce-144.
To separate Ce-144 from other rare earths, the nitric acid solution from the previous step was percolated through a DOWEX 1x8 (100 - 200 mesh) resin column containing lead dioxide (PbO_2) mixed with the resin. The size and flow rate were the same as mentioned for the AMD column.
Cerium, oxidized to the tetravalent state, remained fixed on the resin together with Pu traces during the subsequent washing step with 8 M HNO_3.

The solution containing rare earths and transplutonium elements was evaporated to dryness and the residue dissolved in 0.05 M hydrochloric acid (0.5 ml). Selective separation of neodymium from its neighbouring rare earths and Am-241, was carried out utilizing the method described by L. Koch and coworkers [3]. The 0.05 M HCl solution was percolated through a DOWEX 50x8 (200 - 400 mesh) resin column (0.3 cm internal diameter and 6.5 cm long) with a flow rate of 0.013 ml/min. The column was then washed with 0.05 M HCl (0.2 ml) and water (0.15 ml). Rare earths were then eluted with 0.05 M alpha-hydroxy-isobutirric acid (7 ml) at pH = 4.6 and collected in 0.5 ml fractions.

In order to identify the fractions containing only neodymium isotopes, an additional sample spiked with Nd-147 was purified at the same time together with the unknown samples. The 530 KeV gamma photopeak of Nd-147 and scintillation gamma ray spectrometry were utilized to locate, in the sequence of collected fractions, the position of the fractions containing only Nd-147; in a similar way it was possible to identify, and subsequently to combine, the corresponding unknown fractions containing only neodymium isotopes.

After adjustment to 1.5 M HNO_3, the combined neodymium fractions were adsorbed on a DOWEX 50x8 (200 - 400 mesh) resin column (0.55 cm internal diameter, 3 cm long) with a flow rate of about 0.5 ml/min. After washing with 1.5 M HNO_3

(4 ml), the neodymium was eluted with 6 M HNO_3 (3 ml).

The neodymium solution was then evaporated to dryness and the residue redissolved in 1 M HNO_3 in order to have a suitable solution for M.S. analyses (20-40 ug Nd/g). A total of seven samples were purified for each dissolved cross section; three unspiked, three Nd-150 spiked plus one Nd-147 spiked.

5.1.4. Mass spectrometry.

At the Ispra laboratory, mass spectrometric measurements have been performed on uranium, plutonium and neodymium. The mass spectrometric measurements were carried out on instruments (Varian Mat type CH4 and AEI MS-503) equipped with thermal-ionization double filament sources for most of the experiments. Only a part of neodymium determinations were performed with ion sources in a single filament arrangement. The mass spectra were obtained by the scanning of the analyzing magnet current.

For all of the fuel samples, three spiked and three unspiked, independently purified solutions have been prepared. In general, the third solution of each group was analyzed only in case of a poor agreement in the results; for each fuel sample a minimum of two mass spectrometric runs for the different types of solutions were carried out. Finally for each run the number of scans of the isotopes group was at least equal to ten.

Corrections have been introduced for mass discrimination effects as determined by isotopic standards of the National Bureau of Standards (USA).

The ratios of the minor isotopes to the most abundant one (e.g. U-234, U-235, U-236 to U-238 and Pu-240, Pu-241, Pu-242 to Pu-239) determined at the Ispra and Karlsruhe Research Centers are reported in Table 12, together with their relative

Table 12 : Isotopic atom ratio of uranium and plutonium.

ASSEM-BLY	ROD	AXIAL LOCAT.	MEASURED VALUES											
			235/238	RSD	236/238	RSD	234/238	RSD	240/239	RSD	241/239	RSD	242/249	RSD
G-7		1	0.02068	0.5	0.00170	1.0	0.000136	1.0	0.1421	0.6	0.0466	1.0	0.0043	2.5
		4	0.01597	0.5	0.00256	1.8	0.000152	1.5	0.2218	0.6	0.0975	0.8	0.0166	1.8
		4K	0.01573	1.1	0.00254	4.6			0.22295	0.2	0.10064	0.4	0.01769	2.6
		9	0.01844	0.4	0.00221	1.0	0.000163	2.6	0.1758	0.4	0.0666	0.8	0.0080	2.0
		9K	0.01823	0.2	0.00214	0.8			0.1786	0.4	0.0686	0.3	0.0086	0.5
	2	1	0.01945	0.7	0.00186	1.5	0.000144	3.0	0.1546	0.8	0.0522	1.1	0.0053	2.0
		4	0.01466	0.5	0.00263	2.0	0.000139	3.0	0.2423	0.9	0.1064	1.1	0.0211	2.5
		7K	0.01463	1.0	0.00270	1.4			0.2417	0.3	0.1067	0.5	0.0213	1.1
		9K	0.01748	0.5	0.00224	2.6			0.1931	0.4	0.0740	0.7	0.0103	0.8
	3	1	0.01938	0.3	0.001847	0.4	0.000148	1.5	0.1646	0.4	0.0578	0.65	0.0064	1.0
		1K	0.02015	0.7	0.001810	2.2			0.1512	0.3	0.0478	0.4	0.0045	2.9
		7	0.01409	0.45	0.00281	0.7	0.000173	1.5	0.2592	0.4	0.1166	1.2	0.0250	2.0
		7K	0.01428	0.7	0.00281	1.6			0.2555	0.3	0.1153	0.4	0.0267	0.8
		9	0.01698	0.3	0.00233	0.8	0.000139	1.0	0.2020	0.6	0.0805	1.5	0.0115	1.8
H-10	4	1	0.02451	0.4	0.00171	2.5	0.000223	3.5	0.1265	0.7	0.0405	0.9	0.0034	3.0
		4	0.01831	0.6	0.00299	2.0	0.000246	3.0	0.2115	0.4	0.0962	0.9	0.0162	1.3
		7	0.01760	0.6	0.00289	1.5	0.000150	3.0	0.2163	0.7	0.0974	0.8	0.0179	2.0
		9	0.02129	0.6	0.00263	1.5			0.1747	0.4	0.0690	0.9	0.0085	3.0
	5	4K	0.01773	0.4	0.00315	0.7			0.2332	1.0	0.1079	0.4	0.0205	1.3
		7	0.0173	0.6	0.00320	2.0	0.000160	3.0	0.2372	0.5	0.1094	0.8	0.0209	1.5
		9	0.0202	0.6	0.00255	1.5	0.000180	3.0	0.1867	0.5	0.0760	1.2	0.10	2.5
	6	7	0.01593	0.6	0.00328	2.0	0.000125	3.0	0.2600	0.6	0.1157	1.2	0.0257	2.0
L-7	7	7	0.02811	0.45	0.00288	0.8			0.1555	0.8	0.0627	1.0	0.0068	2.0
		7K	0.02858	0.5	0.00292	1.1			0.1563	0.3	0.0629	0.5	0.0067	1.0
	8	1	0.0370	0.5	0.00124	2.0	0.000230	3.0	0.0630	0.6	0.0080	1.2	0.0003	3.5
		7	0.0327	0.6	0.00204	2.0	0.000210	3.0	0.1154	0.4	0.0265	0.8	0.0018	3.0

K = KARLSRUHE LABORATORY

standard deviations.

The concentrations of uranium and plutonium nuclides have been determined by means of the isotopic dilution techniques, utilizing as spiking isotopes, U-233 and Pu-242. The spike solutions were calibrated against standards of the National Bureau of Standards with a relative error in the concentration values between 0.3 and 0.5%, which includes also the uncertainties due to the isotope dilution procedures.

The concentration of Nd-148, the chosen burnup indicator, was determined again by the isotopic dilution technique with Nd-150 as a spike. A correction has been introduced for the contamination due to natural neodymium on the basis of the determination of Nd-142.

The presence of Ce-142 and Sm-150 has been verified and suitable corrections have been introduced by taking into account the peaks at masses 140 due to cerium, 149 and 152 due to samarium. The spike solution of Nd-150 has been calibrated against a standard of natural neodymium supplied by the Central Bureau of Nuclear Measurements of Euratom in Geel. The error in the calibration, inclusive of the uncertainties due to the isotope dilution procedures, was between 0.6 and 0.8%.

The plutonium/uranium and Nd-148/uranium ratios are reported in Table 13, together with the relative percentual differences for the pairs of adjacent pellets analyzed at Ispra and Karlsruhe laboratories. The U and Pu isotopic ratios for these adjacent pellets and the relative percentual differences between the two laboratories are reported in Table 14. The agreement between the two groups of data is satisfactory with the exception of the sample G 7-3-1. This deviation may be due to the severe power and temperature gradients, because independent measurements of uranium and plutonium isotopic

Table 13 : Plutonium/Uranium and Nd-148/Uranium mass ratios.

SAMPLE	Pu/U x 10^{-3}			Nd-148/U x 10^{-4}		
	ISPRA	KARLSRUHE	Δ %	ISPRA	KARLSRUHE	Δ %
G-7-1-1	4.362					
G-7-1-4	6.895	6.857	0.6	1.619	1.657	2.3
G-7-1-9	5.179	5.316	2.6		1.160	
G-7-2-1	4.437			0.992		
G-7-2-4	6.698			1.688		
G-7-2-7		6.921			1.737	
G-7-2-9		5.479			1.268	
G-7-3-1	4.412	4.183	5.2	1.012	0.889	12.1
G-7-3-7	6.913	7.016	1.4		1.774	
G-7-3-9	5.464			1.374		
H-10-4-1	4.131			0.824		
H-10-4-4	7.151			1.760		
H-10-4-7	7.157			1.821		
H-10-4-9	5.638			1.315		
H-10-5-4		7.234			1.896	
H-10-5-7	7.355			1.998		
H-10-5-9	5.735			1.411		
H-10-6-7	7.168			2.063		
L-7-7-7	5.601	5.657	1.0	1.361	1.390	2.1
L-7-8-1	1.577			0.390		
L-7-8-7	2.920			0.865		

Table 14 : Comparison of the results for uranium and plutonium isotopic atom ratios obtained at Karlsruhe and Ispra laboratories.

SAMPLE	U-235/U-238	Δ%	U-236/U-238	Δ%	Pu-240/Pu-239	Δ%	Pu-241/Pu-239	Δ%	Pu-242/Pu-239	Δ%
G-7-1-4	I 0.01597	1.5	I 0.00256	0.7	I 0.2218	0.5	I 0.0975	3.1	I 0.0166	6.2
	K 0.01573		K 0.00254		K 0.2230		K 0.1006		K 0.0177	
G-7-1-9	I 0.01844	1.1	I 0.00221	3.3	I 0.1758	1.6	I 0.0666	2.9	I 0.0080	7.0
	K 0.01823		K 0.00214		K 0.1786		K 0.0686		K 0.0086	
G-7-3-1	I 0.01938	3.8	I 0.00185	2.0	I 0.1646	8.1	I 0.0578	17.3	I 0.0064	29.7
	K 0.02015		K 0.00181		K 0.1512		K 0.0478		K 0.0045	
G-7-3-7	I 0.01409	1.3	I 0.00281	0	I 0.2592	1.4	I 0.1166	1.1	I 0.0250	6.4
	K 0.01428		K 0.00281		K 0.2555		K 0.1153		K 0.0267	
L-7-7-7	I 0.02811	1.6	I 0.00288	1.4	I 0.1555	0.5	I 0.0627	0.3	I 0.0068	1.5
	K 0.02858		K 0.00292		K 0.1563		K 0.0629		K 0.0067	

compositions, as well as plutonium/uranium and Nd-148/uranium ratios, show a disagreement in the same sense.

A detailed description of the mass spectrometry procedures utilized at Karlsruhe can be found in Reference [2]. In addition to the mass spectrometric measurements on uranium, plutonium and neodymium, the Karlsruhe laboratory has also performed isotopic composition measurements on americium and fission gases. The results obtained for americium and fission gases are reported in Table 15 and 16.

5.1.5. Alpha spectrometry.

The alpha spectrometry measurements have been carried out only at the Transuranium Institute of Karlsruhe. Without any chemical treatment, an aliquot of the fuel solution containing about 0.01 mg of uranium was dropped onto a counting plate. The alpha spectrum was taken by means of a semiconductor silicon detector, connected through an amplifier, to a multichannel analyzer.

The alpha decay energies partly overlap, so that only the activity ratios (Pu-238 + Am-241)/(Pu-239 + Pu-240), Cm-242/(Pu-239 + Pu-240) and Cm-244 / (Pu-239 + Pu-240) can be determined. By measuring the (Pu-239 + Pu-240) / Pu-238 activity ratio in the sample purified for mass spectrometry, and by using the ratio Pu-239/Pu-240 determined by mass spectrometry, the concentrations of the single nuclides can be computed. The accuracy of the method is about 2-5%.
More details can be found in Reference [2].
The results of the alpha spectrometry measurements are reported in Table 17.

Table 15 : Americium isotopic atom ratios.

SAMPLE	$\frac{Am-242}{Am-241}$	$\frac{Am-243}{Am-241}$
G-7-1-4	0.00351 ± 13.5%	0.06886 ± 1.99%
G-7-1-9	0.00282 ± 12.4%	0.03585 ± 1.30%
G-7-2-7	0.00271 ± 7.22%	0.08032 ± 1.34%
G-7-2-9		0.04068 ± 3.44%
G-7-3-1	0.00323 ± 5.50%	0.01793 ± 2.07%
G-7-3-7	0.00340 ± 5.93%	0.08806 ± 1.04%
H-10-5-4	0.00239 ± 6.11%	0.08006 ± 1.58%
L-7-7-7	0.00205 ± 4.45%	0.03050 ± 1.67%

Table 16 : Krypton and xenon isotopic atom ratios

SAMPLE	KRYPTON			XENON		
	83/86	84/86	85/86	131/134	132/134	136/134
G-7-1-4	0.2571 ± 0.66 %	0.5639 ± 0.30 %	0.0947 ± 0.39 %	0.3281 ± 0.64 %	0.6619 ± 0.29 %	1.4062 ± 0.27 %
G-7-1-9	0.2672 ± 0.07 %	0.5665 ± 0.17 %	0.1082 ± 1.22 %	0.3406 ± 1.45%	0.6393 ± 0.65 %	1.351 ± 0.43 %
G-7-2-7	0.2550 ± 1.94 %	0.5628 ± 1.93 %	0.1043 ± 1.59 %	0.3295 ± 0.19 %	0.6660 ± 0.17 %	1.4292 ± 0.13 %
G-7-2-9	0.2613 ± 0.61 %	0.5555 ± 0.32 %	0.1063 ± 0.36 %	0.3416 ± 0.22 %	0.6396 ± 0.23 %	1.3659 ± 0.26 %
G-7-3-1	0.2667 ± 1.08 %	0.5478 ± 1.02 %	0.1084 ± 1.10 %	0.3523 ± 0.30 %	0.6170 ± 0.30 %	1.2953 ± 0.23 %
G-7-3-7	0.2552 ± 0.45 %	0.5716 ± 0.39 %	0.1048 ± 0.44 %	0.3240 ± 0.36 %	0.6656 ± 0.12 %	1.4476 ± 0.16%
H-10-5-4	0.2547 ± 1.02 %	0.5649 ± 0.70 %	0.1057 ± 0.87 %	0.3248 ± 0.52 %	0.6659 ± 0.14 %	1.4025 ± 0.53 %
L-7-7-7	0.2657 ± 0.04 %	0.5520 ± 0.21 %	0.1051 ± 0.13 %	0.3387 ± 0.75 %	0.6334 ± 0.30 %	1.2800 ± 0.07 %

Table 17 : Percent of activity for alpha-emitting nuclides of plutonium, americium and curium.

SAMPLE	BEFORE SEPARATION				AFTER SEPARATION	
	Pu-239+240 %	Pu-238+Am-241 %	Cm-242 %	Cm-244 %	Pu-239+240 %	Pu-238 %
G-7-1-4	32.72 ± 0.73 %	57.17 ± 0.33 %	1.49 ± 2.79 %	8.61 ± 1.58 %	49.77	50.23
G-7-1-9	42.57 ± 0.18%	51.31 ± 0.84%	1.91 ± 0.56 %	4.21 ± 5.9 %	59.0	41.0
G-7-2-7	31.06 ± 1.32%	59.44 ± 0.92%	2.72 ± 5.78 %	6.78 ± 2.51 %	47.56	52.44
G-7-2-9	41.50 ± 0.7 %	51.86 ± 0.44%	1.48 ± 17.6 %	5.14 ± 9.0 %	60.03	39.97
G-7-3-1	51.50 ± 0.70%	45.57 ± 0.87%	0.74 ± 17 %	2.19 ± 16.4 %	72.89	27.11
G-7-3-7	31.09 ± 1.28%	57.50 ± 0.97%	1.69 ± 8.84 %	9.72 ± 4.94 %	46.32	52.68
H-10-5-4	30.60 ± 0.92 %	58.70 ± 0.56%	2.54 ± 13.4 %	8.17 ± 5.16 %	45.24	54.76
L-7-7-7	40.64 ± 0.88 %	54.74 ± 0.65%	0.78 ± 19.21%	3.84 ± 9.31 %	57.11	42.89

5.2. Processing of the experimental data and theoretical predictions.

The processing of the experimental results and the theoretical predictions have been carried out by FIAT NUCLEARE in the framework of the EURATOM-FIAT contract n° 098-66-6 TEEI. In the present report only a short description is given of the codes utilized for the interpretation of the experimental data and the prediction of the results. Complete information can be found in Ref. [4], [5] and [6].

5.2.1. Processing of the experimental data.

The code developed for the interpretation of the results is the BURNUP code [7], similar to the REBUF code [8], which has been used to infer the various fuel characteristics from the concentrations of the uranium and plutonium nuclides and of the Cs-137 and Nd-148 fission products.

The main outputs of the BURNUP code are the following :

- The total burnup in MWd/t(U) and the fraction due to each fissionable isotope, calculated from the concentrations of uranium and plutonium nuclides. The burnup dependent parameters :

  α_{49} = capture to fission ratio for Pu-239

  α_{41} = capture to fission ratio for Pu-241

  δ_{28} = ratio of U-238 fissions to U-235, Pu-239, Pu-241 fissions.

  required to evaluate the burnup have been obtained from the PHANTOM code [9], which has also been utilized for the calculation of the energy release per fission for different burnup levels.

The values of energy release per fission, utilized in the calculations, are the following :

U-235	199.8 MeV	U-236	199.8 MeV	U-238	197.3 MeV
Pu-239	207.2 MeV	Pu-240	207.2 MeV	Pu-241	209.3 MeV

- The burnup in MWd/t(U) calculated from the Cs-137concentrations. The following Cs-137 nuclear data have been utilized in the calculations :

  half life 30.5 y

  fission yields % [11][12]

U-235	6.28	U-238	6.30
Pu-239	6.74	Pu-241	6.60

  The average fission yield and the average energy release per fission have been calculated from the fractions of each isotopic fission.

- The burnup in MWd/t(U) calculated from the Nd-148 concentrations. The following Nd-148 nuclear data have been utilized for the calculations :

  fission yields % [10][11]

U-235	1.69	U-238	1.93
Pu-239	1.70	Pu-241	1.89

  A correction has been introduced for the Nd-148 losses due to neutron capture, using a resonance integral of 18.7 b and a 2200 m/sec absorption cross section of 2.54 b. The correction rose to 1% at the maximum burnup of the samples analysed.

- The net production and depletion of uranium and plutonium isotopes relative to the initial uranium loading. An initial concentration has been assumed for U-236 on the basis of the known values [12] for other fuels of almost the same enrichment. The code performs corrections for the decay of Pu-241 and for the neutron capture by U-236 and Pu-242.

5.2.2. Theoretical predictions.

The detailed evaluation of burnup and isotopic inventory characteristics within the core has been performed using :

- a full core representation in X, Y geometry in order to obtain the average characteristics of the fuel assemblies and of the fuel rods under examination ;
- a simplified multichannel synthesis technique for the estimation of the axial shapes along the fuel assemblies or fuel rods under examination and of the local burnup and isotopic inventory at the sample positions.

Three basic computer codes have been used for the detailed spatial burnup evaluation.

The PHANTOM [9], a unit cell spectrum dependent burnup evaluation code :

- provides the initial number densities and the burnup dependent microscopic cross section libraries for input to one and two dimensional few group diffusion-depletion codes ;
- evaluates the macroscopic group constants for structural materials explicitly represented in the diffusion codes;
- provides fuel nuclear parameters for input to BURNUP data reducing code ;
- provides survey calculations to evaluate the consistency of the measured data.

The CONDOR-3 [13], a two dimensional 20,000 meshes diffusion theory pointwise depletion code is used in X, Y geometry to represent in detail the average cross section of the full core. The results have been interpreted in terms of burnup and isotopic inventory in each fuel assembly or fuel rod and in each different enrichment region.

The SQUIRREL [14], a one dimensional diffusion-depletion code, accounting for local variation of moderator and fuel

temperature is used to :

- estimate the transverse leakage as a function of burnup to be adopted in X, Y calculations ;
- evaluate the axial burnup and isotopic inventory in each fuel assembly or fuel rod examined using radial buckling, local power and control rod poisoning as obtained from CONDOR-3.

5.3. Analysis of the experimental results and comparison with theoretical predictions.

The experimental results concerning burnup, heavy isotopes and fission products have been analysed in order to evaluate their consistency, following three different procedures.

- Five pairs of adjacent fuel sections have been analysed at Ispra and Karlsruhe. The comparison between the experimental results of the two laboratories are reported in section 5.1. for Cs-137 and Nd-148 contents, uranium and plutonium ratios and isotopic compositions. In the present section a comparison is performed between the burnup values calculated from the experimental data of the two laboratories, to provide a check of the results.
- The burnup values have been determined by means of different techniques. A comparison between independently determined burnup values allows a check of the validity of the results.
- Linear correlations between different nuclides in irradiated fuels and between nuclides and burnup parameters have been experimentally observed [2][15][16]. These correlations can be utilized for a check of the experimental data. In fact, the observation of a linear correlation between two sets of independent data is a proof of their consistency. Several linear correlations, observed by plotting the experimental data, are presented as a demonstration of the validity of the results.

In the second part of this section, the experimental values of burnup and production and depletion of uranium and plutonium nuclides have been compared with the theoretical predictions. A similar comparison can be found in References [5] and [6].

5.3.1. Analysis of the experimental results.

5.3.1.1. Comparison between burnup values.

Table 18 summarizes, for the different burnup determination techniques, the nuclear data and codes utilized for processing the experimental data and indicates the estimated errors.

The errors due to the values of energy release per fission are not included. For the Cs-137 technique two values are reported for the estimated errors, the first one being related to the destructive measurements, the second one to the non-destructive determination. The errors have been evaluated by quadratic combination of the errors in the measurements and in the nuclear data. For instance in the case of the Cs-137 technique, there are three main sources of error :

1) Error in the reference source used for the Cs-137 determination.
2) Statistical error of the measurement.
3) Error in the nuclear data for half-life and fission yields.

The results of the measurements on the five adjacent fuel sections, analyzed at Ispra and Karlsruhe, are compared in Table 19.

The agreement of the results is very satisfactory (within 4%) with the exception of the samples G-7-3-1. For these samples a disagreement in the same sense was observed also for the measurements of isotopic compositions and plutonium/uranium ratios. This fact supports the opinion that the deviation does

Table 18 : Techniques used for the burnup determination from experimental data.

Technique	Required Nuclear Data*	Required Codes	Error %
Cs-137	Half-life and fission yields of Cs-137	PHANTOM Code BURNUP Code	4 - 5
Nd-148	Fission yields and neutron capture cross sections of Nd-148	PHANTOM Code BURNUP Code	2
Heavy elements	Cross sections for neutron fission and capture of heavy elements	PHANTOM Code BURNUP Code	4

*The values of energy release per fission, utilized in the calculations, are the following :

U-235	199.8 MeV	U-236	199.8 MeV	U-238	197.3 MeV
Pu-239	207.2 MeV	Pu-240	207.2 MeV	Pu-241	209.3 MeV

Table 19 : Burnup values -MWd/t(U)- obtained by different experimental techniques. Comparison between results obtained at Ispra and Karlsruhe.

Technique / Sample	Cs-137			Nd-148			Heavy elements		
	Ispra	Karlsruhe	Diff. %	Ispra	Karlsruhe	Diff. %	Ispra	Karlsruhe	Diff. %
G-7-1-4	14099	13883	+ 1.5	14155	14490	- 2.4	14193	14441	- 1.7
G-7-1-9	10478	10444	+ 0.3				10200	10544	- 3.3
G-7-3-1	8879	7716	+13.1	8895	7814	+12.1	9103	8052	+11.5
G-7-3-7	16146	15740	+ 2.5				16648	16460	+ 1.1
L-7-7-7	12035	12242	- 1.7	11912	12172	- 2.2	12381	11906	+ 3.8

not derive from experimental errors but from a real difference in the burnup of the adjacent pellets.

Table 20 shows the values of all the burnup measurements performed at Ispra and Karlsruhe with different techniques. In all, 26 fuel samples have been analysed.

The burnup values obtained by different techniques are in close agreement. In fact, if the averages of the different experimental determinations are taken and the standard deviations are calculated, these latter range from 1% to 4% for all of the samples with the exception of the samples L-7-8-1, which have a standard deviation of about 7%. These differences are within the limits of errors of the different methods reported in Table 18.

In Table 21 the burnup values obtained with Cs-137 and Nd-148 are compared in order to investigate possible systematic differences, which could be produced by the cesium migration.

The values obtained with Cs-137 are in most cases lower than the values obtained with Nd-148. However, if the average is taken of all the determinations, the burnup value from Cs-137 is only 1% lower than the burnup value from Nd-148. A difference of this magnitude can be explained by the uncertainties in the nuclear data, mainly in the fission yields. Consequently, the cesium migration can be excluded.

The agreement between the results obtained in different laboratories and derived from different techniques has shown that complete confidence may be placed in the validity of the experimental burnup values and in the estimated errors of the measurements.

Table 20 : Burnup values -MWd/t(U)- obtained by different experimental techniques.

Assembly	Rod	Axial Location	Cs-137 non destr.	Cs-137 destr.		Heavy elements		Nd-148	
			Ispra	Ispra	Karlsruhe	Ispra	Karlsruhe	Ispra	Karlsruhe
G-7	1	1	7987	7822	-	7677	-	-	-
		4*	14645	14099	13883	14193	14411	14155	14490
		9*	11252	10478	10444	10200	10544	-	10187
	2	1	8584	8307	-	8897	-	8713	-
		4	15024	14644	-	15730	-	14770	-
		7	15442	-	15007	-	15731	-	15193
		9	10706	-	11142	-	11410	-	11127
	3	1*	8509	8879	7716	9103	8052	8895	7814
		7*	16531	16146	15740	16648	16460	-	15506
		9	11324	11860	-	12065	-	12053	-
H-10	4	1	7340	7415	-	7932	-	7243	-
		4	14697	15156	-	15680	-	15377	-
		7	15251	15477	-	16616	-	15898	-
		9	12119	11226	-	11457	-	11529	-
	5	4	16719	-	16400	-	16624	-	16556
		7	16885	17064	-	17132	-	17450	-
		9	12415	12219	-	12837	-	12366	-
	6	7	18613	17715	-	18697	-	17995	-
L-7	7	7*	12606	12035	12242	12381	11906	11912	12172
	8	1	3236	3717	-	3211	-	3435	-
		7	7327	7411	-	7152	-	7605	-

* pairs of adjacent fuel sections

Table 21 : Comparison between burnup values -MWd/t(U)- determined by means of Cs-137 and Nd-148.

Assembly	Rod	Axial location	Cs-137		Nd-148		Difference %	
			Ispra	Karlsruhe	Ispra	Karlsruhe	Ispra	Karlsruhe
G-7	1	4	14099		14155		-0.4	
		4		13883		14490		-4.4
		9		10444		10178		+2.5
	2	1	8307		8713		-4.9	
		4	14644		14770		-0.9	
		7		15007		15493		-1.2
		9		11142		11127		+0.1
	3	1	8879		8895		-0.2	
		7		15740		15506		+1.5
		9	11860		12053		-1.6	
H-10	4	1	7415		7243		+2.3	
		4	15156		15377		-1.5	
		7	15477		15898		-2.7	
		9	11226		11529		-2.7	
	5	4		16400		16556		-1.0
		7	17064		17450		-2.3	
		9	12219		12366		-1.2	
	6	7	17715		17995		-1.6	
L-7	7	7	12035		11912		+1.0	
		7		12242		12172		+0.6
	8	1	3717		3435		+7.6	
		7	7411		7605		-2.6	

5.3.1.2. Correlations.

Several correlations have been observed between different nuclides in irradiated fuels and between nuclides and burnup values. These correlations are an important tool for checking the validity of the experimental data. Some of these correlations seem to be useful also for more general problems of fissile material management and nuclear safeguards.

First of all it seems interesting to correlate the burnup data, which have been previously checked by various comparisons, with one of the fundamental quantities, the U-235/U-238 isotopic ratio. The experimental burnup data (averages of all the determinations with different techniques) are plotted versus the U-235/U-238 ratio in Fig. 29. The experimental points are distributed on three straight lines corresponding to the different initial enrichments. Linear correlations are also observed in Fig. 30, where the U-235/U-238 ratio is plotted versus the Pu-240/Pu-239 ratio.

Fig. 29 and 30 provide a check of the two most important isotopic ratios determined in the post-irradiation analysis.

Interesting results have also been obtained for the correlations between fission products and heavy nuclides or burnup values.

The study on the correlations between gaseous fission products and heavy nuclides, which is conducted by the Transuranium Institute [16], has been continued through the analyses of the fission gases in 8 fuel samples.

Fig. 31 shows a linear correlation between uranium depletion (D_5) and Kr-84/Kr-83 atom ratio, which seems to be independent of the initial enrichment. The parameters of the least square straight line are very similar to the parameters obtained for other reactors [16].

In Fig. 32 the Xe-131/Xe-134 ratio is plotted versus the Pu/U ratio. Also this correlation seems to be independent of the initial enrichment.

Isotope correlations between radioactive fission products and heavy nuclides have been carefully investigated at Ispra utilizing the results of the post-irradiation analyses.
In Fig. 33 the Cs-137, Ce-144 and Ru-106 specific activities are plotted versus the Pu/U mass ratios. The relationships between fission product activities and Pu/U mass ratios seem to be linear over a range of Pu/U mass ratio between 4×10^{-3} and 8×10^{-3} corresponding to a burnup range between 7,500 and 18,000 MWd/t(U). The 2 points with the lowest burnup values do not fit the least square lines. It has to be noted that the corresponding fuel pellets have been taken from a rod (L-7-8) positioned at the periphery of the core where the neutron spectrum is extremely perturbed.
In Fig. 34 the Cs-134/Cs-137 activity ratio is plotted versus Pu/U mass ratio.
In Fig. 35 the Cs-134/Cs-137 activity ratio is plotted versus the burnup expressed in MWd/t(U). Also in these cases linear correlations are observed.

The parameters obtained in the regression analysis of the above reported correlationsare shown in Tables 22 and 23.

The observed correlations prove the consistency of the experimental data which will be compared in the next section with the theoretical predictions.

The isotope correlations seem to be useful also for other problems of the fuel cycle, mainly for the verification of the uranium and plutonium data obtained during the reprocessing operations. The correlations between plutonium and radioactive fission products suggest also the possibility of non-destructive measurements of the plutonium content in irradiated fuels.

Table 22 : Results of the regression analysis.

Correlation y	x	Correlation Coefficient	Regression equation	Standard error of regression coeff.	Standard error of regression coefficient %
Burnup versus	U-235/U-238 Enr. 2.72%	- 0.993	$Y = -0.1343 \cdot 10^{7} x + 0.3507 \cdot 10^{5}$	$0.4478 \cdot 10^{5}$	3.3
	U-235/U-238 Enr. 3.13%	- 0.993	$Y = -0.1268 \cdot 10^{7} x + 0.3851 \cdot 10^{5}$	$0.6033 \cdot 10^{5}$	4.8
	U-235/U-238 Enr. 3.89%	- 0.997	$Y = -0.1014 \cdot 10^{7} x + 0.4087 \cdot 10^{5}$	$0.4998 \cdot 10^{5}$	4.9
U-235/U-238	vs. $Pu\text{-}240/_{Pu\text{-}239}$ Enr. 2.72%	- 0.996	$Y = -0.5647 \cdot 10^{-1} x + 0.2847 \cdot 10^{-1}$	$0.1367 \cdot 10^{-2}$	2.4
	vs. $Pu\text{-}240/_{Pu\text{-}239}$ Enr. 3.13%	- 0.988	$Y = -0.6466 \cdot 10^{-1} x + 0.3241 \cdot 10^{-1}$	$0.4186 \cdot 10^{-2}$	6.5
	vs. $Pu\text{-}240/_{Pu\text{-}239}$ Enr. 3.89%	- 0.980	$Y = -0.6856 \cdot 10^{-1} x + 0.3943 \cdot 10^{-1}$	$0.9698 \cdot 10^{-2}$	14.1
$(W_5^\circ - W_5)/W_5^\circ$	vs. Kr-84/Kr-83	0.988	$Y = 0.1145 \cdot 10^{1} x - 0.2071 \cdot 10^{1}$	$0.7432 \cdot 10^{-1}$	6.5
Pu/U	" Xe-133/Xe-134	- 0.990	$Y = -0.1081 \quad x + 0.4229 \cdot 10^{-1}$	$0.6356 \cdot 10^{-2}$	5.9
Pu/U	" Cs-137	0.979	$Y = 0.4512 \cdot 10^{-10} x + 0.1735 \cdot 10^{-2}$	$0.2521 \cdot 10^{-11}$	5.6
Pu/U	" Ru-106	0.963	$Y = 0.8623 \cdot 10^{-11} x + 0.2432 \cdot 10^{-2}$	$0.6395 \cdot 10^{-12}$	7.4
Pu/U	" Ce-144	0.967	$Y = 0.3981 \cdot 10^{-11} x + 0.4166 \cdot 10^{-3}$	$0.2814 \cdot 10^{-12}$	7.1
Pu/U	" Cs-134/Cs-137	0.991	$Y = 0.6318 \cdot 10^{-2} x + 0.9301 \cdot 10^{-3}$	$0.2233 \cdot 10^{-3}$	3.5
Burnup	" Cs-134/Cs-137	0.988	$Y = 0.1828 \cdot 10^{5} x - 0.1697 \cdot 10^{4}$	$0.7444 \cdot 10^{3}$	4.1

Table 23 : Errors of the regression estimate.

Correlation y	x		$\bar{x}$	$\bar{y}$	Standard error about the regression(*)	S.E. about the regres. Mean $\bar{y}$ %	S.E. of the regression estimate in the range of the experimental data % (**)
Burnup	versus U-235/U-238	Enr. 2.72%	$0.1715 \cdot 10^{-1}$	$0.1203 \cdot 10^{5}$	$0.3700 \cdot 10^{3}$	3.1	0.82 - 2.55
		Enr. 3.13%	$0.1911 \cdot 10^{-1}$	$0.1429 \cdot 10^{5}$	$0.4405 \cdot 10^{3}$	3.1	1.09 - 4.85
		Enr. 3.89%	$0.3160 \cdot 10^{-1}$	$0.8828 \cdot 10^{4}$	$0.3593 \cdot 10^{3}$	4.1	2.03 - 9.69
U-235/U-238	vs. Pu-240/Pu-239	Enr. 2.72%	0.2004	$0.1715 \cdot 10^{-1}$	$0.1993 \cdot 10^{-3}$	1.2	0.31 - 0.70
		Enr. 3.13%	0.2058	$0.1911 \cdot 10^{-1}$	$0.4669 \cdot 10^{-3}$	2.4	0.86 - 1.80
		Enr. 3.89%	0.1143	$0.3160 \cdot 10^{-1}$	$0.9970 \cdot 10^{-3}$	3.1	1.58 - 2.22
$(W_5^\circ - W_5)/W_5^\circ$	"	Kr-84/Kr-83	$0.2154 \cdot 10^{1}$	0.3963	$0.1360 \cdot 10^{-1}$	3.4	1.21 - 3.15
Pu/U	"	Xe-131/Xe-134	0.3349	$0.6083 \cdot 10^{-2}$	$0.1670 \cdot 10^{-3}$	2.7	0.97 - 2.97
Pu/U	"	Cs-137	$0.9215 \cdot 10^{8}$	$0.5893 \cdot 10^{-2}$	$0.2462 \cdot 10^{-3}$	4.2	1.04 - 2.75
Pu/U	"	Ru-106	$0.4014 \cdot 10^{9}$	$0.5893 \cdot 10^{-2}$	$0.3217 \cdot 10^{-3}$	5.5	1.36 - 3.93
Pu/U	"	Ce-144	$0.1376 \cdot 10^{10}$	$0.5893 \cdot 10^{-2}$	$0.3076 \cdot 10^{-3}$	5.2	1.30 - 3.20
Pu/U	"	Cs-134/Cs-137	0.7856	$0.5893 \cdot 10^{-2}$	$0.1577 \cdot 10^{-3}$	2.7	0.67 - 1.78
Burnup	"	Cs-134/Cs-137	0.7856	$0.1266 \cdot 10^{5}$	$0.5258 \cdot 10^{3}$	4.1	1.04 - 2.82

* $$\sigma = \sqrt{\frac{\sum_{i=1}^{n}(y_i-\bar{y})^2 - b^2 \sum_{i=1}^{n}(x_i-\bar{x})^2}{n-2}} = \sqrt{\frac{\sum_{i=1}^{n}(y_i-Y_i)^2}{n-2}}$$

** $$S.E.(Y_k) = \sigma \sqrt{\frac{1}{n} + \frac{(x_k-\bar{x})^2}{\sum_{i=1}^{n}(x_i-\bar{x})^2}}$$

where y = experimental values
Y = values predicted from the regression line
n = number of observations

5.3.2. Comparison between experimental data and theoretical predictions.

The comparison between experimental and theoretical burnup values is shown in Table 24, where the experimental values are the average of the results obtained with different techniques. The agreement is extremely good for all the samples with the exception of the samples in the extreme position 1 and 9. In fact for the samples taken from the other positions the maximum deviation between theoretical and experimental values is 2.3%. The difference of 18% for the sample H-10-4-1 can be explained with the presence of the neighbouring control rod. The difference of 12% for the sample L-7-8-1 can be explained by a poor representation of the water reflectors. In fact, the rod L-7-8 is placed at the periphery of the core.

In Table 25 the burnup values, determined in 48 points by non-destructive Cs-137 measurements, are compared with the theoretical predictions.

Some comments have to be made regarding this comparison :

- the axial locations 2, 4 and 8 of rod number 8 correspond to flux depressions due to the fuel former, detected by gross gamma-scanning. The experimental values are lower than the theoretical values because the calculations do not take into account these local flux depressions.
- The agreement is very good for the axial locations 4 and 7.
- Near the upper and the lower ends of the fuel rods the agreement is less pronounced.

The comparison between experimental and theoretical values of the rod average burnup is shown in Table 26. The experimental rod average burnup has been calculated from the burnup measured at a few points utilizing the theoretical axial distribution.

Table 24 : Comparison between experimental and theoretical burnup values -MWd/t(U)- . The experimental values are the average of the results obtained by different techniques.

Assembly	Rod	Axial Location	Exper. Value	Theoretical Value	Difference %
G-7	1	1	7829	8091	-3.3
		4	14268	14034	+1.6
		9	10517	11049	-5.0
	2	1	8625	8727	-1.2
		4	15042	15137	-0.6
		7	15343	15358	-0.1
		9	11096	11826	-6.6
	3	1 *	8846	8997	-1.7
		7	16172	16307	-0.8
		9	11825	12653	-7.0
H-10	4	1	7482	8301	-17.6
		4	15227	15098	+0.8
		7	15810	15492	+2.0
		9	11583	12392	-7.0
	5	4	16575	16381	+1.2
		7	17133	16809	+1.9
		9	12459	13251	-6.3
	6	7	18255	17916	+1.8
L-7	7	7	12179	11903	+2.3
	8	1	3399	3000	+11.7
		7	7374	7500	-1.7

* Samples examined at Ispra Laboratories

Table 25 : Comparison between experimental and theoretical burnup values -MWd/t(U)-

M = non-destructive Cs-137 measurements

P = theoretical predictions

Assembly	G-7						H-10						L-7			
Rod	1		2		3		4		5		6		7		8	
Axial Location	M	P	M	P	M	P	M	P	M	P	M	P	M	P	M	P
1	7987	8091	8584	8727	8509	8997	7340	8301	8486	9549	9547	10178	5639	6741	3236	3000
2	12345	12203	12489	13162	13165	13875	12619	13156	13403	14275	13051	15214	7719	9955	4783	5350
4	14645	14034	15024	15137	16118	16072	14697	15098	16719	16381	16790	17460	11910	11415	6514	7030
7	14400	14239	15442	15358	16531	16307	15251	15492	16885	16809	18613	17916	12606	11903	7327	7500
8	14107	13651	15040	14724	15098	15634	14996	15018	13957	16294	16943	17367	11539	11626	6112	7200
9	11252	11049	10706	11826	11324	12653	12119	12392	12415	13251	13741	14330	8749	9621	4941	5600

Table 26 : Rod average burnup. Comparison between experimental and theoretical values -MWd/t(U)-.

Rod Number	Experimental values	Theoretical values	Differences %
1	12930	13239	-3.4
2	11996	12274	-2.3
3	13475	14057	-4.3
4	12913	13353	-3.4
5	14372	14488	-0.8
6	15550	15442	+0.7
8	6288	6073	+3.4

The good agreement between theoretical and experimental values (maximum difference 4.3%) indicates that the difference observed for the extreme positions of the rods have a small influence on the rod average burnup.

The comparisons between experimental and theoretical values of isotopic production and depletion are reported in Fig. 36, 37 and 38 for the inner, intermediate and outer core regions respectively. The curves of Pu-239, Pu-240, Pu-241 and U-236 production and U-235 and U-238 depletion as a function of the burnup have been obtained by means of the CONDOR-3 code. The points represent the experimental values. Data obtained from asymptotic, intermediate and perturbed spectra are indicated with different symbols. The agreement between theoretical and experimental values appears to be quite satisfactory. Also the deviations which can be observed for samples taken from perturbed spectra are in the expected directions. In the case of the Pu-239 production the experimental points from the perturbed rods always lie below the theoretical curve. This fact can be explained by the spectrum variation due to the water gap.

The comparison between experimental and theoretical values of the U-235 depletion and U-236 production is shown in Table 27. Also in this case the maximum differences are observed for the samples H-10-4-1 and L-7-8-1. If the values of these two sections are neglected, the average of the differences between experimental and theoretical values is about 3.5% for the U-235 depletion and about 2.5% for the U-236 production. If the average of all the determinations is considered the differences are only 1.5% and 1.2% for the U-235 depletion and for the U-236 production respectively.

The comparison between experimental and theoretical values of the Pu-239, Pu-240 and Pu-241 production is shown in Table 28.

Table 27 : Comparison between experimental and theoretical values of U-235 depletion and U-236 production -kg/t(U)-.

ASSEMBLY	ROD	Axial Location	D 25 exp.	D 25 calc.	Diff. %	P 26 exp.	P 26 calc.	Diff. %
G-7	1	1	7.47	7.84	- 5.0	1.430	1.519	- 6.2
		4 (I)	12.05	12.22	- 1.4	2.240	2.285	- 2.0
		4 (K)	12.28	12.22	+ 0.5	2.220	2.285	- 2.9
		9 (I)	9.64	10.22	- 6.1	1.915	1.928	- 0.7
		9 (K)	9.84	10.35	- 5.2	1.847	1.950	- 5.6
	2	1	8.65	8.75	- 1.2	1.583	1.604	- 1.3
		4	13.29	12.92	+ 2.8	2.306	2.332	- 1.1
		7	13.33	13.09	+ 1.8	2.371	2.435	- 2.7
		9	10.56	11.01	- 4.3	1.942	2.034	- 4.7
	3	1	8.71	9.38	- 7.6	1.570	1.606	- 2.3
		7 (I)	13.85	13.71	+ 1.0	2.475	2.497	- 0.9
		7 (K)	13.67	13.71	- 0.3	2.484	2.497	- 0.5
		9	11.04	11.73	- 6.3	2.027	2.087	- 3.0
H-10	4	1	8.01	8.81	-10.0	1.434	1.732	-20.8
		4	14.02	13.70	+ 2.3	2.636	2.623	+ 0.5
		7	14.69	14.02	+ 4.6	2.541	2.647	- 4.2
		9	11.13	11.82	- 6.2	2.304	2.254	+ 2.2
	5	4	14.58	14.56	+ 0.1	2.786	2.758	+ 1.0
		7	14.99	14.86	+ 0.9	2.832	2.805	+ 1.0
		9	12.41	12.63	- 1.7	2.214	2.363	- 6.7
	6	7	16.28	15.64	+ 3.9	2.907	2.867	+ 1.4
L-7	7	7 (I)	12.56	12.06	+ 4.1	2.520	2.355	+ 6.5
		7 (K)	12.13	12.06	+ 0.6	2.558	2.355	+ 8.6
	8	1	3.948	3.45	+14.4			
		7	8.09	8.80	- 9.2			

TABLE 28 : Comparison between experimental and theoretical values of Pu-239, Pu-240, Pu-241 production -kg/t(U)-

ASSEMBLY	ROD	AXIAL LOCATION	P 49 exp.	P 49 calc.	Diff. %	P 40 exp.	P 40 calc.	Diff. %	P 41 exp.	P 41 calc.	Diff. %
G-7	1	1	3.608	3.972	-10.1	0.515	0.577	-12.1	0.204	0.185	- 9.0
		4 (I)	5.041	5.248	- 4.1	1.123	1.101	+ 2.0	0.596	0.584	+ 1.9
		4 (K)	4.991	5.248	- 5.1	1.118	1.101	+ 1.5	0.609	0.584	+ 4.0
		9 (I)	4.072	4.548	-11.7	0.719	0.853	-18.7	0.329	0.351	- 6.9
		9 (K)	4.159	4.588	-10.3	0.746	0.869	-16.5	0.346	0.363	- 5.1
	2	1	3.606	3.952	- 9.6	0.560	0.630	-12.6	0.228	0.205	+10.2
		4	4.769	5.220	- 9.5	1.160	1.202	- 3.6	0.615	0.646	- 5.1
		7	4.926	5.154	- 4.6	1.196	1.220	- 2.0	0.637	0.651	- 2.3
		9	4.134	4.505	- 9.0	0.802	0.923	-15.1	0.371	0.382	- 3.0
	3	1 (I)	3.537	3.410	+ 3.6	0.585	0.644	-10.2	0.248	0.188	+23.9
		7 (I)	4.806	4.532	+ 5.7	1.251	1.292	- 3.3	0.679	0.642	+ 5.5
		7 (K)	4.889	4.532	+ 7.3	1.254	1.292	- 3.0	0.683	0.642	+ 6.1
		9	4.141	3.978	+ 3.9	0.840	0.986	-17.4	0.404	0.383	+ 5.2
H-10	4	1	3.483	4.158	-19.4	0.442	0.580	-31.1	0.171	0.197	-15.4
		4	5.266	5.479	- 4.0	1.118	1.101	+ 1.5	0.614	0.617	- 0.5
		7	5.234	5.426	- 3.7	1.137	1.129	+ 0.7	0.618	0.635	- 2.8
		9	4.418	4.824	- 9.2	0.775	0.890	-14.9	0.369	0.400	- 8.4
	5	4	5.172	5.457	- 5.5	1.211	1.205	+ 0.5	0.676	0.682	- 0.8
		7	5.234	5.404	- 3.2	1.247	1.237	+0.8	0.694	0.702	- 1.2
		9	4.446	4.765	- 7.2	0.834	0.959	-15.0	0.409	0.429	- 4.8
	6	7	4.968	4.620	+ 7.0	1.297	1.313	- 1.2	0.697	0.666	+ 4.4
L-7	7	7 (I)	4.647	4.549	+ 2.1	0.723	0.676	+ 6.5	0.350	0.305	+14.8
		7 (K)	4.525	4.549	- 0.5	0.710	0.676	+ 5.0	0.345	0.305	+13.1
	8	1	1.464	1.22	+20.0						
		7	2.525	2.540	- 0.6						

For the Pu-239 production the agreement is within 10% with the exception of the samples H-10-4-1 and L-7-8-1. If the values of these samples are neglected, the average of the differences is about 6%. The calculated values of the Pu-239 production are normally higher than the experimental values. If the average of all the determinations is considered, the calculated value is 3.5% higher than the experimental value.

The same overestimation is observed for the Pu-240 production. The average of the theoretical values is about 6% higher than the average of the experimental values.

The same overestimation of the plutonium production is observed in the comparison between theoretical data and experimental data obtained during the reprocessing operations of the Trino Vercellese fuel elements in the Eurochemic plant [5].

This deviation is mainly due to an overestimation of the effective fuel temperature and consequently of the Doppler effect (the fuel temperature was considered constant during burnup). Two PHANTOM calculations performed, one with constant fuel temperature and the other with variable fuel temperature during burnup show a reduction of the fissile plutonium production of 2.5% in the second calculation.

6. CONCLUSION.

The post-irradiation analysis of the TRINO VERCELLESE fuel elements indicates that the used theoretical evaluation methods of the burnup and of the concentration of heavy atoms are quite satisfactory.

The comparison of the experimental results with the theoretical data leads to the following conclusions :

- A very good agreement was observed for the local burnup values in all positions with the exception of those near the upper and lower ends of the fuel rods, where the agreement is less satisfactory.

- The rod average burnup is predicted with a good precision.

- With regard to the isotopic concentration of heavy atoms it was observed that the Pu-239 and Pu-240 production are slightly overestimated, whereas the prediction of the U-235 depletion and the U-236 production is in good agreement with the experimental data.

The work performed has also permitted to gain a complete confidence in the experimental techniques through a comparison between the results obtained by different methods and in different laboratories and through an analysis of the experimental data by the isotope correlation technique.
It has been shown that the non-destructive gamma spectrometry can be a relatively simple and useful method for the determination of local burnup in single fuel rods. It demands however a calibration by one of the destructive analyses described.

The programmed post-irradiation examination of one spent fuel assembly, discharged at the end of the second cycle of the Trino Vercellese reactor, will give other interesting results to confirm the reliability of the theoretical predictions.

ACKNOWLEDGEMENTS.

The authors are very grateful to Mr. R. Casini and Mr. Bannella of ENEL for the proposal of the program and for their interest.

REFERENCES

[1] A. COSTANTINO
Report on the Operations Performed at CCR-EURATOM at Ispra on three Irradiated Fuel Assemblies.
ENEL-C3.R1/03/70 (1970).

[2] A. ARIEMMA et al.
Experimental and Theoretical Determination of Burnup and Heavy Isotope Content in a Fuel Assembly Irradiated in the Garigliano Reactor.
Report EUR-4638 (1971).

[3] L. KOCH, G. COTTONE und M.W. GEERLINGS
^{148}Nd Analyse zur Abbrandbestimmung von Kernbrennstoffen.
Radiochim. Acta 10, 122 (1968).

[4] A.M. MONCASSOLI TOSI, P.G. RAMA
Valutazione Dettagliata del Livello di Irraggiamento e della Composizione Locale alla Prima Scarica del Combustibile di Trino Vercellese.
FIAT Report FN-E-117 (1971).

[5] M. DE SERAFINI, A.M. MONCASSOLI TOSI, P.G. RAMA
Trino Vercellese Core One Post-Irradiation Analysis : Interpretation of the Experimental Results and Theoretical Predictions.
FIAT Report FN-E-118 (1971)

[6] A.M. MONCASSOLI TOSI et al.
Post-Irradiation Burnup Analysis of Trino Vercellese Reactor Fuel Elements. Comparison with Theoretical Results.
Paper presented at the Panel of Reactor Burnup Physics, Vienna, 12-16 July 1971. To be published in the Proceedings of the Panel.

[7] G. AROASIO
The BURNUP Code.
EUR Report (in preparation).

[8] R.J. NODVIK
Evaluation of Mass Spectrometric and Radiochemical Analyses of Yankee Core I Spent Fuel.
WCAP 6086 (1966).

[9] L. CRISCUOLO, V. PATERLINI
The PHANTOM Code.
FIAT Nucleare (unpublished).

[10] F.Z. LISMAN et Al.
Burnup Determination of Nuclear Fuel.
Project Report for the Quarter April 1 to June 30, 1968 and Final Report.
IN-1277 (1969).

[11] M.E. MEEK, B.F. RIDER
Summary of Fission Yields for U-235, U-238, Pu-239 and Pu-241 at Thermal Fission Spectra and 14 MeV Neutron Energies
APED-5398 (1968).

[12] R.J. NODVIK
Supplementary Report on Evaluation of Mass Spectrometric and Radiochemical Analyses of Yankee Core I Spent Fuel.
WCAP-6086 (1969).

[13] E. SALINA
CONDOR-3 : A Two-Dimensional Reactor Lifetime Program with Local and Spectrum Dependent Depletion.
Report EUR-4539 (1970).

[14] E. SALINA
The SQUIRREL Code.
FIAT Report FN-E-96 (1969) and EUR Report (in preparation).

[15] D.E. CHRISTENSEN et al.
A Summary of Results Obtained from the First MIST Experiment at Nuclear Fuel Services.
Paper SM-133/54 presented to the IAEA Symposium on Progress in Safeguards Techniques, Karlsruhe, 6-10 July 1970.

[16] L. KOCH, H. BRAUN, A. CRICCHIO
Some Correlations between Isotopes of Xe, Kr, U, Pu and Burnup Parameters for Different Thermal and Fast Reactors.
Paper SM-133/25 presented to the IAEA Symposium on Progress in Safeguards Techniques, Karlsruhe, 6-10 July 1970.

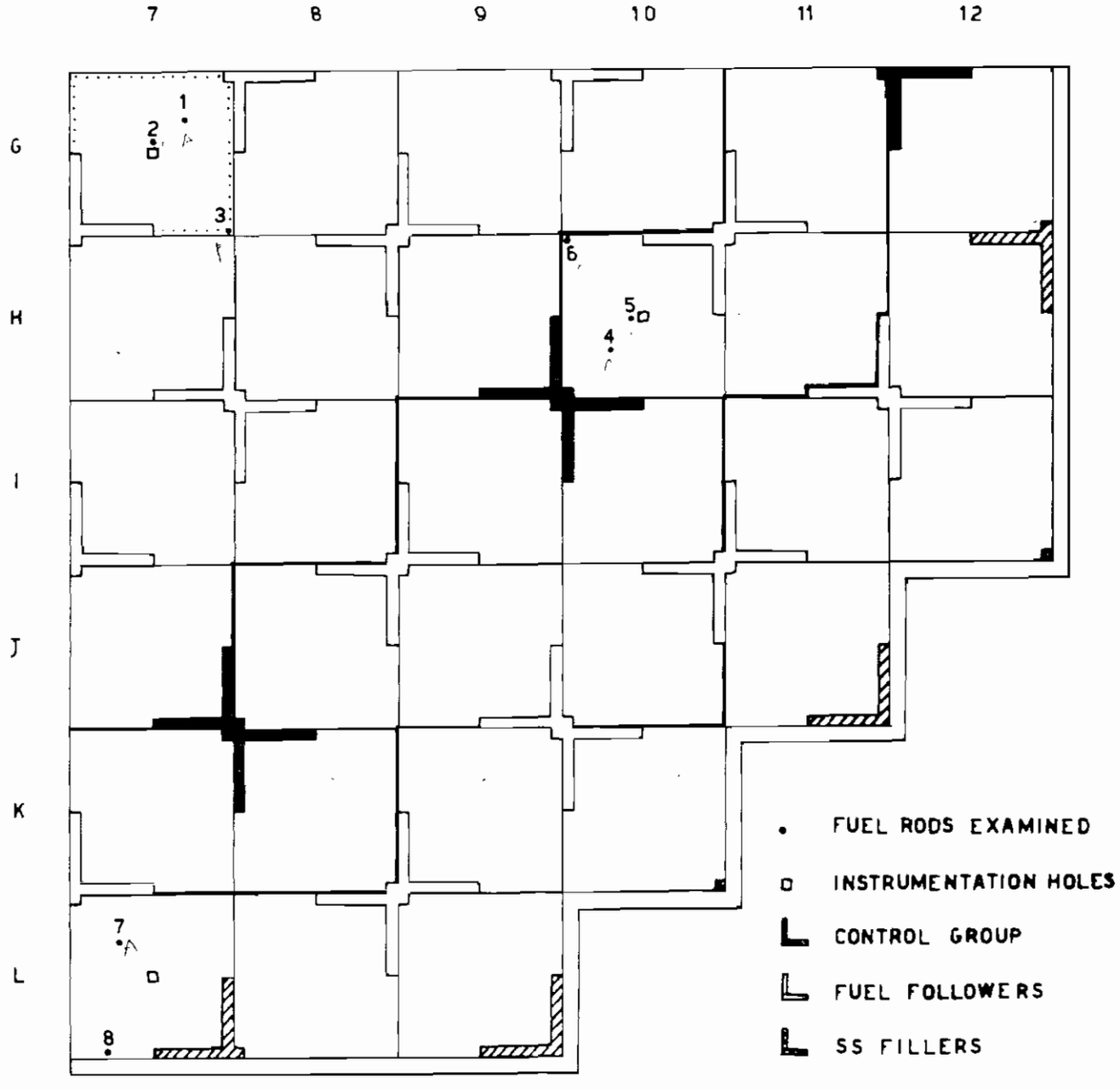

Fig. 1 - S - E quarter core showing location of assemblies dismantled and of rods examined.

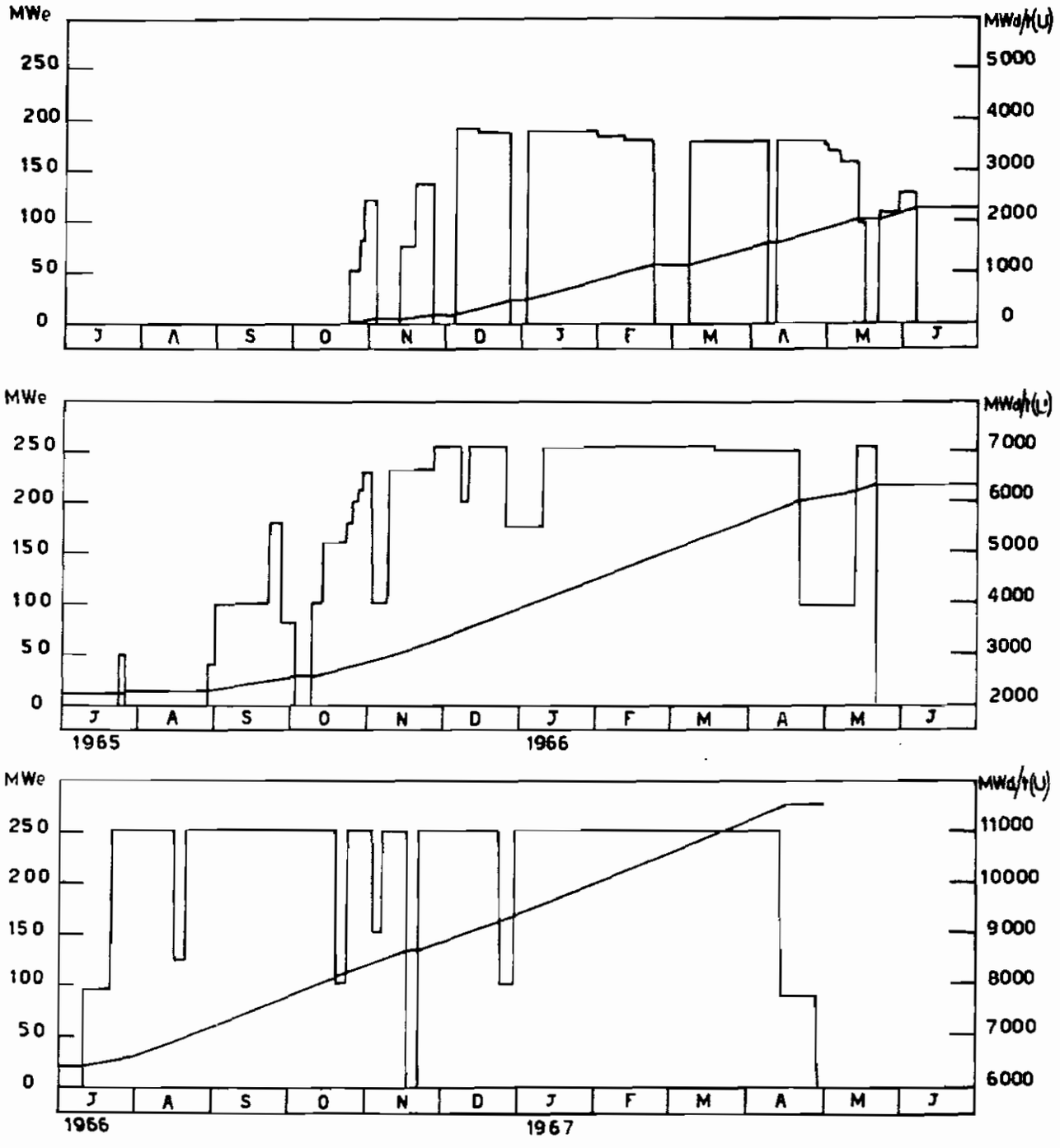

FIG. 2 - Load diagram and cumulative burn-up.

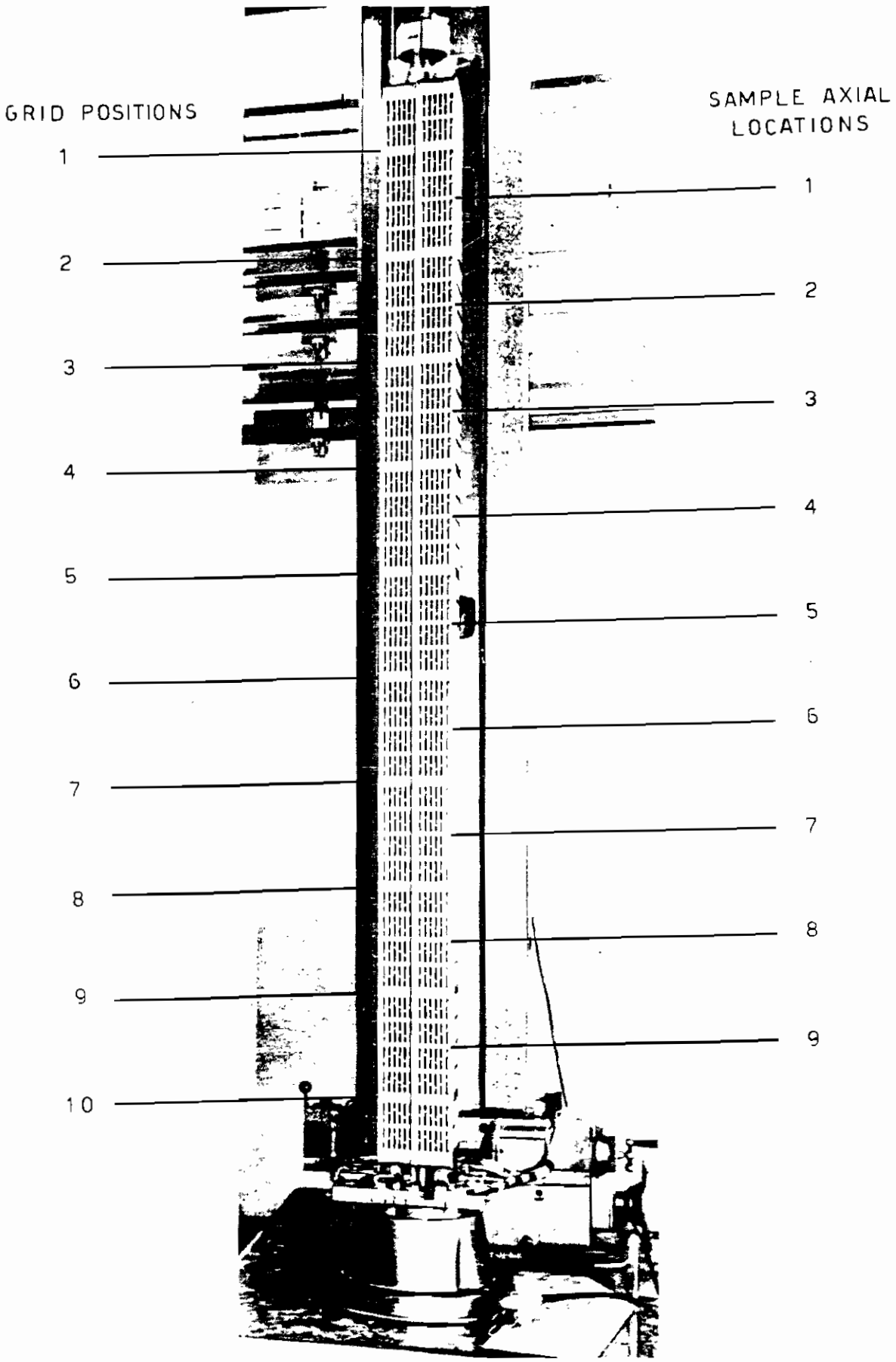

Fig. 3 - Fuel assembly showing positions of grids and axial locations of samples examined.

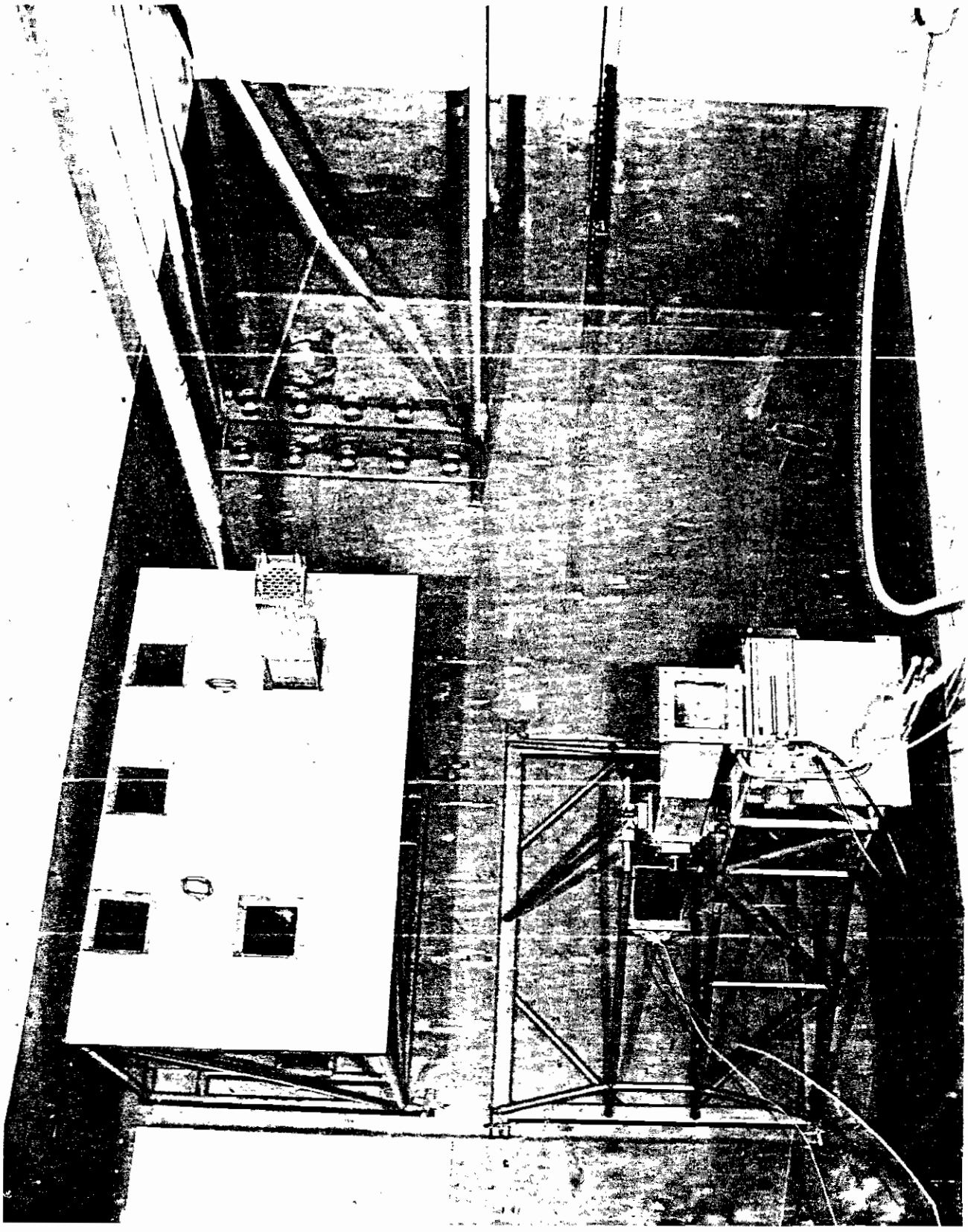

Fig. 4 - Arrangement of the equipment in the pool.

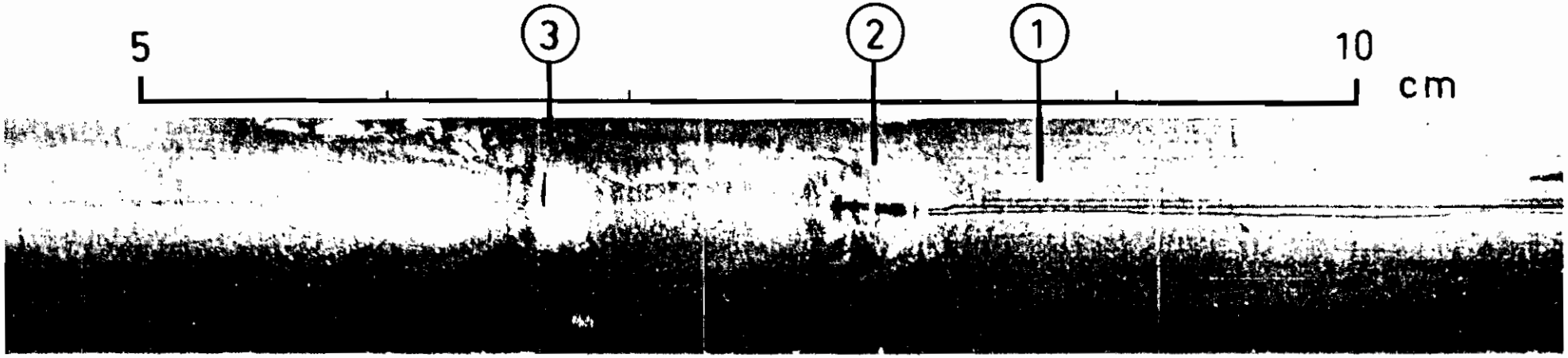

Fig. 5 - Rod No.1 : 1. Black longitudinal scars x 4
2. Mark at spring contact area
3. Halos

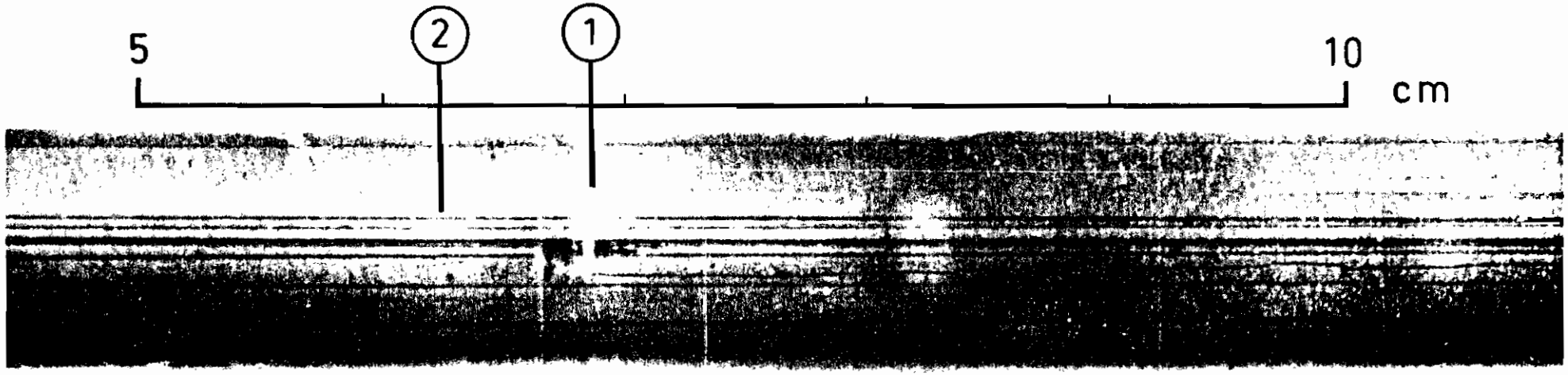

Fig. 6 - Rod No.2 : 1. Mark at spring contact x 4
2. Black longitudinal scars

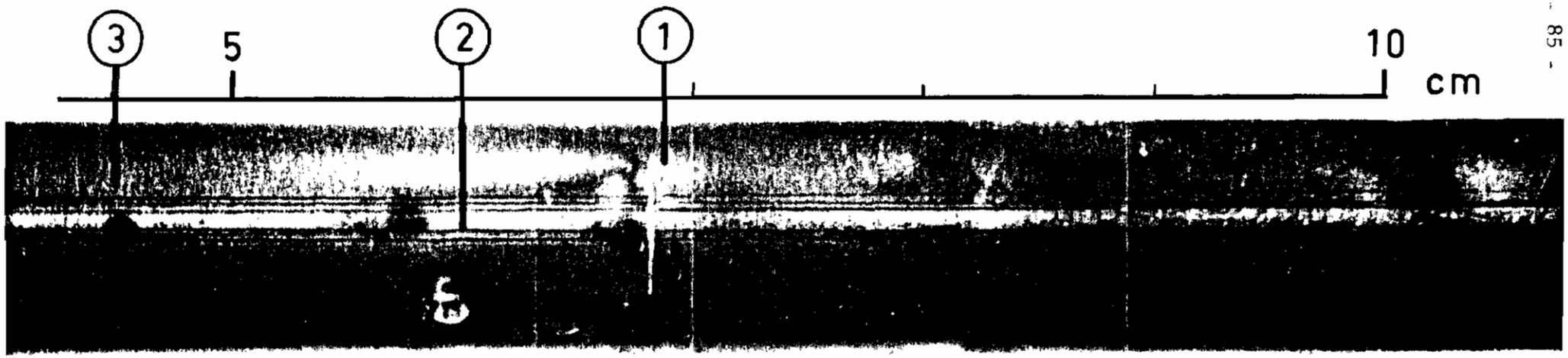

x 4

Fig. 7 - Rod No.7 : 1. Mark at spring contact
2. Circular shape orange colour deposit spot
3. Black spot due to window impurities

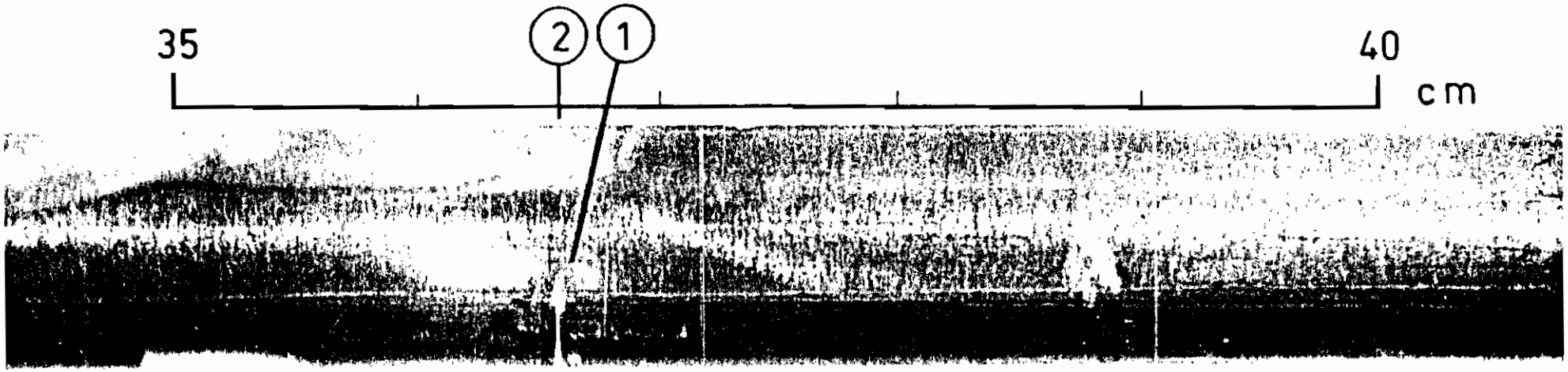

Fig. 8 - Rod No.3 : 1. Glossy mark x 4
2. Water-drop shape, orange colour spot, at spring level

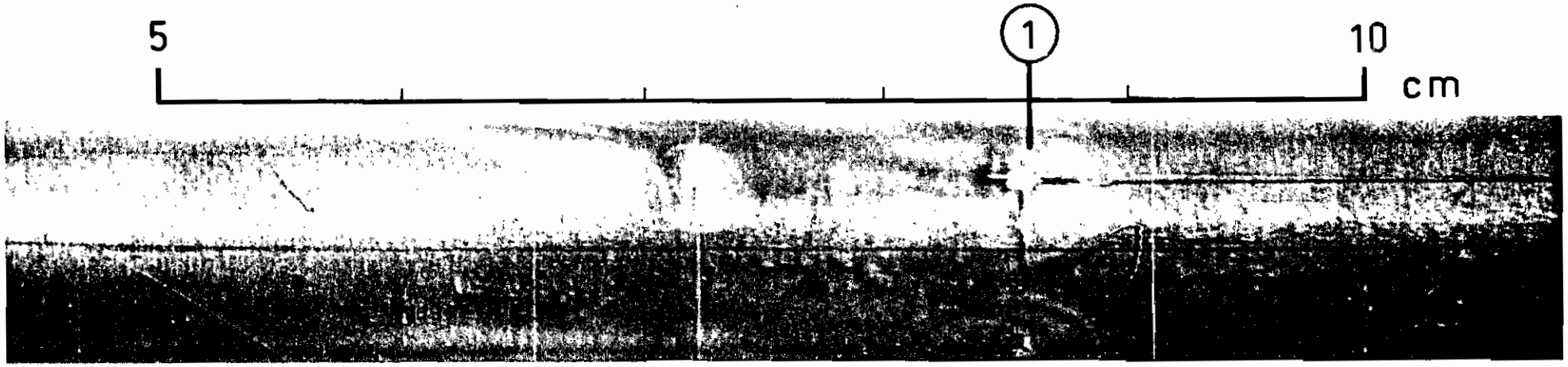

Fig. 9 - Rod No.3 : 1. Glossy marks with fretting corrosion attack

x 4

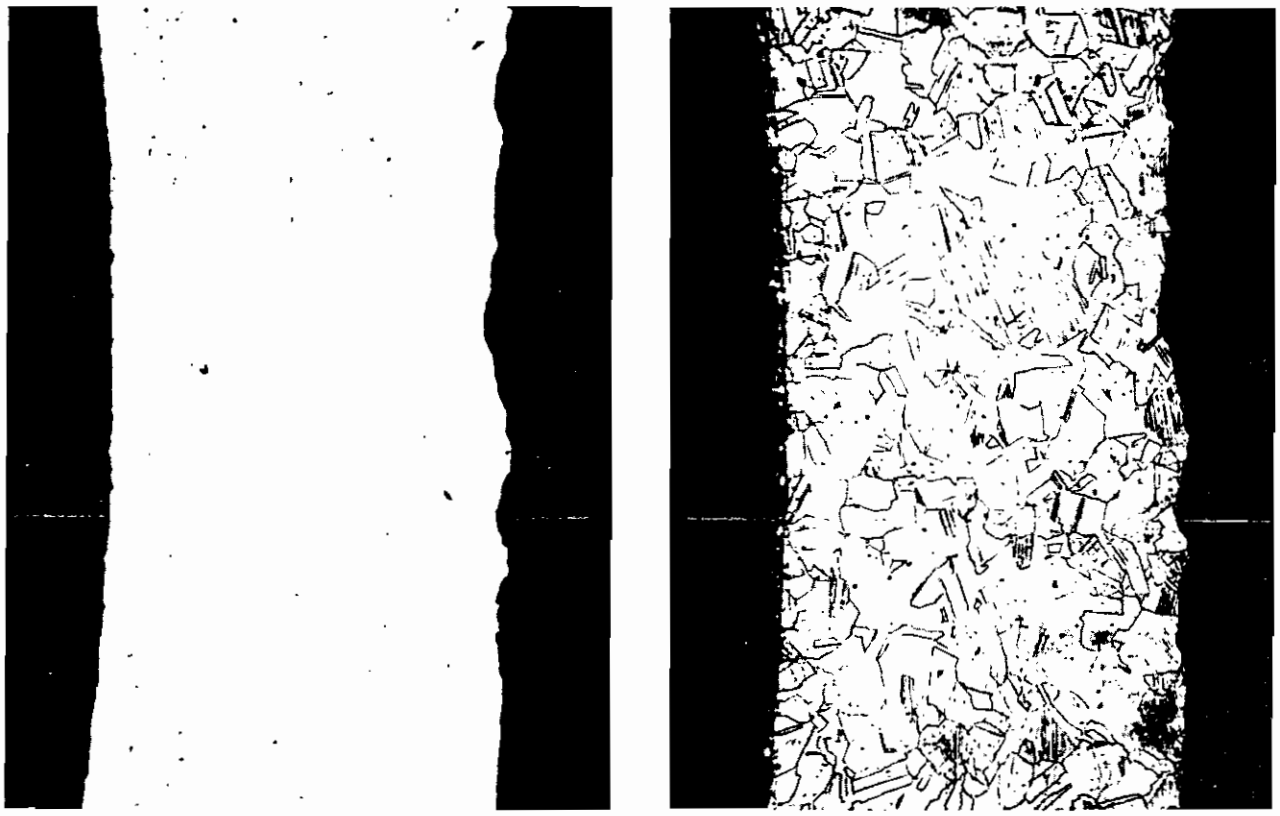

(as polished) (etched)

FIG. 10 - Cross section of the cladding showing a defect produced by fretting corrosion.

x 143

(etched)

FIG. 11 - Cross section of the cladding in the position of a deposit spot shown in Fig. 7.

x 143

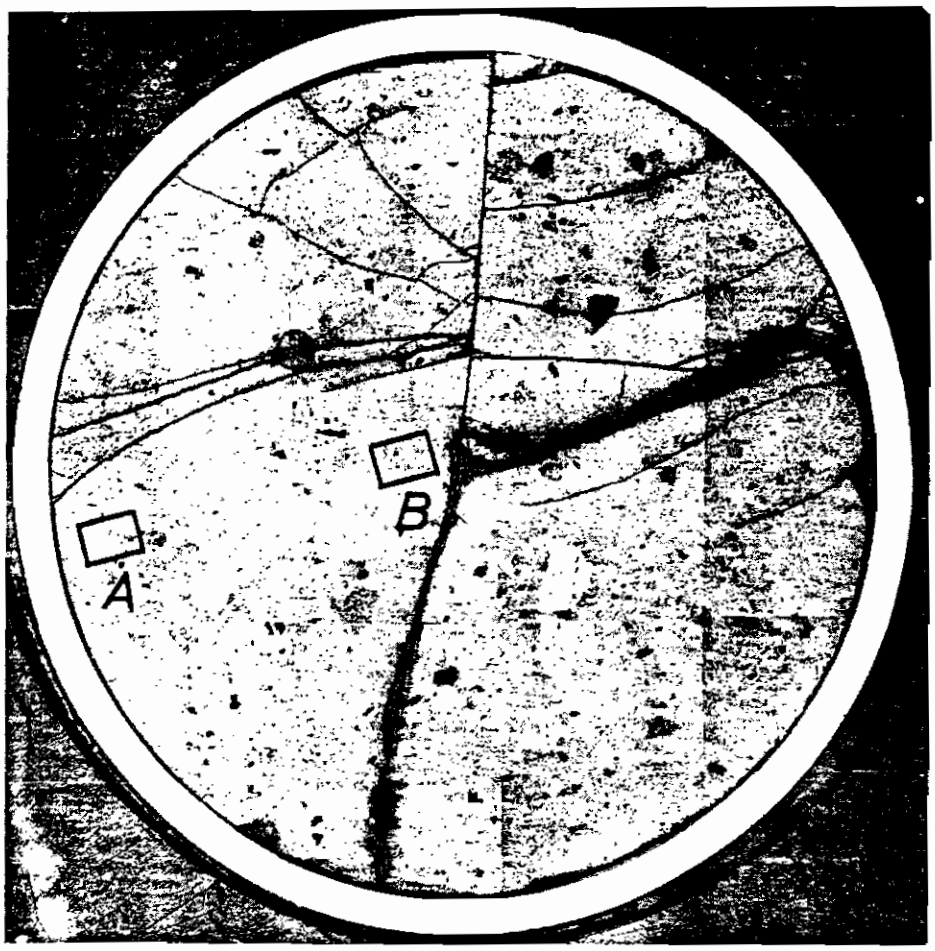

FIG. 12 - Cross section of the fuel rod No.8 (low burnup)
x 12

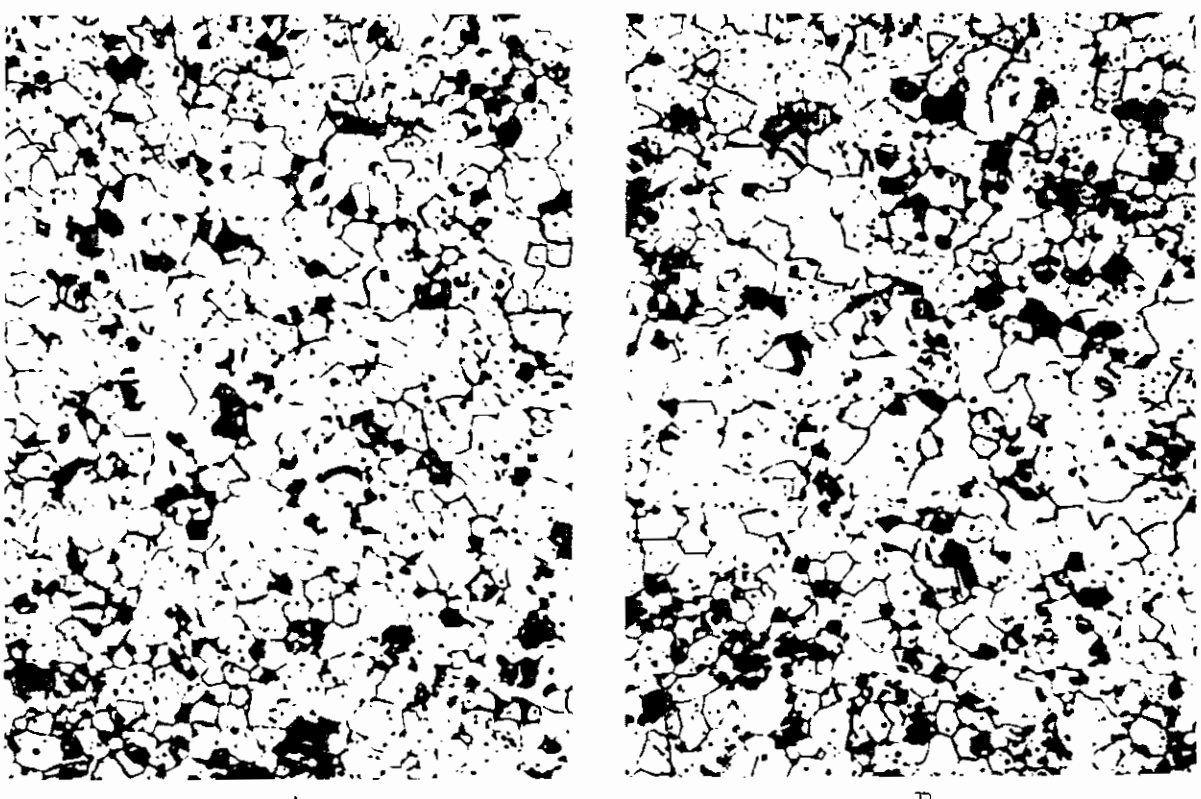

FIG. 13 - Microstructure of the fuel. x 360

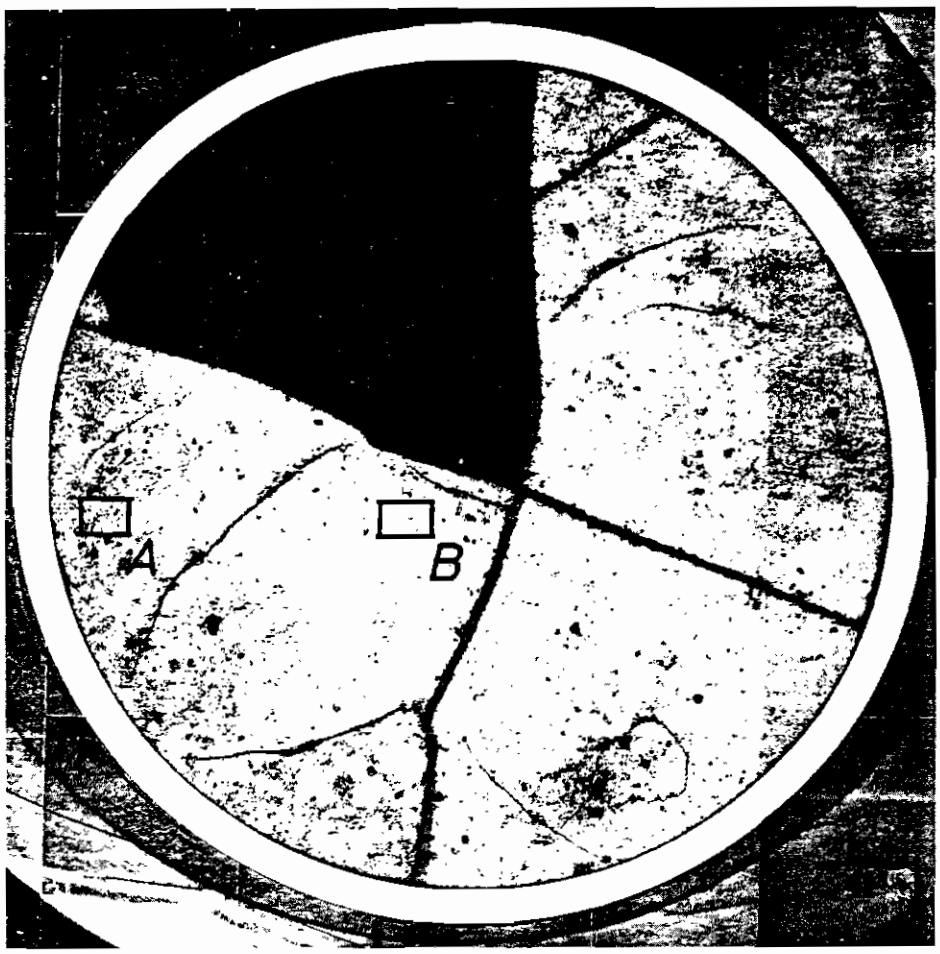

Fig. 14 - Cross section of the fuel rod No.4 (high burnup)
x 12

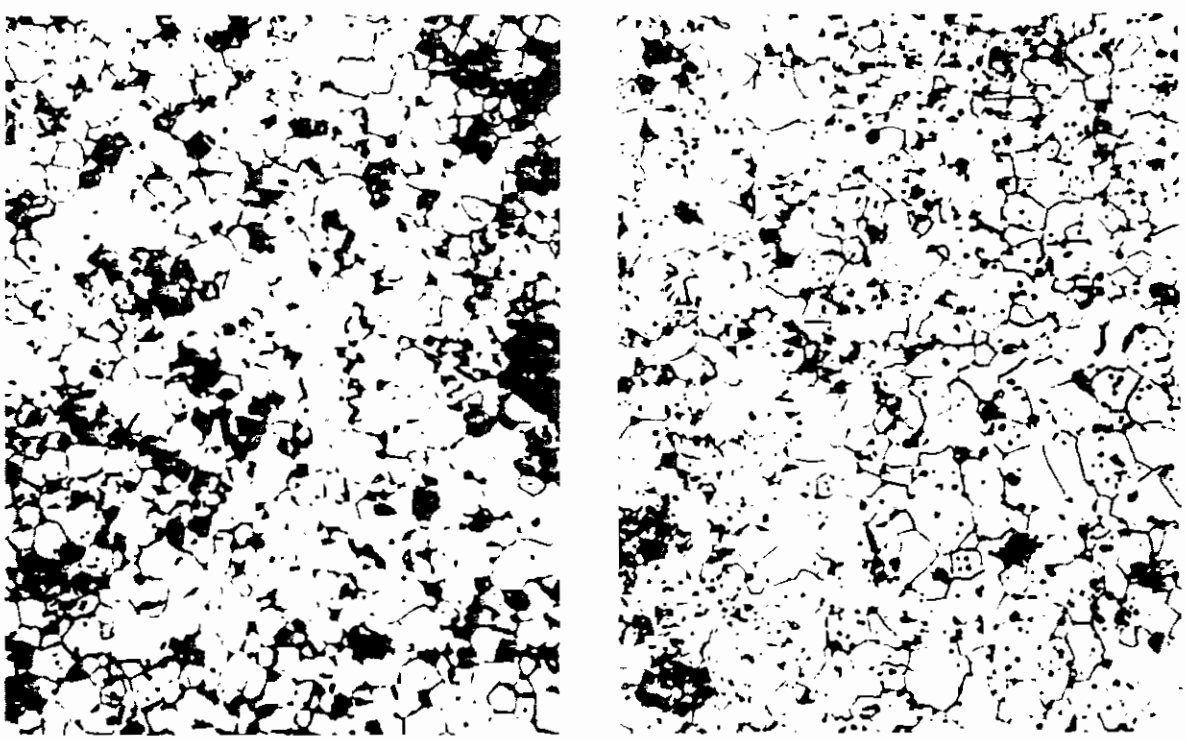

Fig. 15 - Microstructure of the fuel. x 360

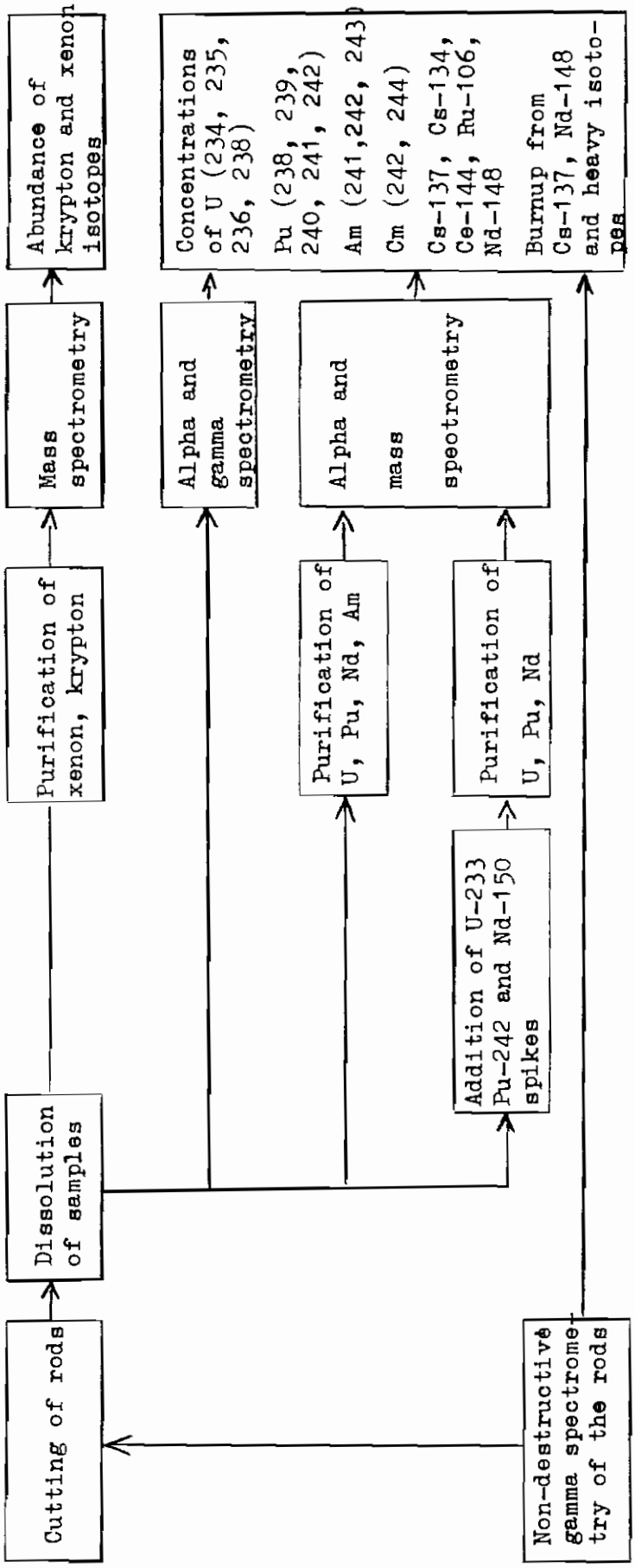

FIG. 16 - Flow diagram of the post-irradiation analyses.

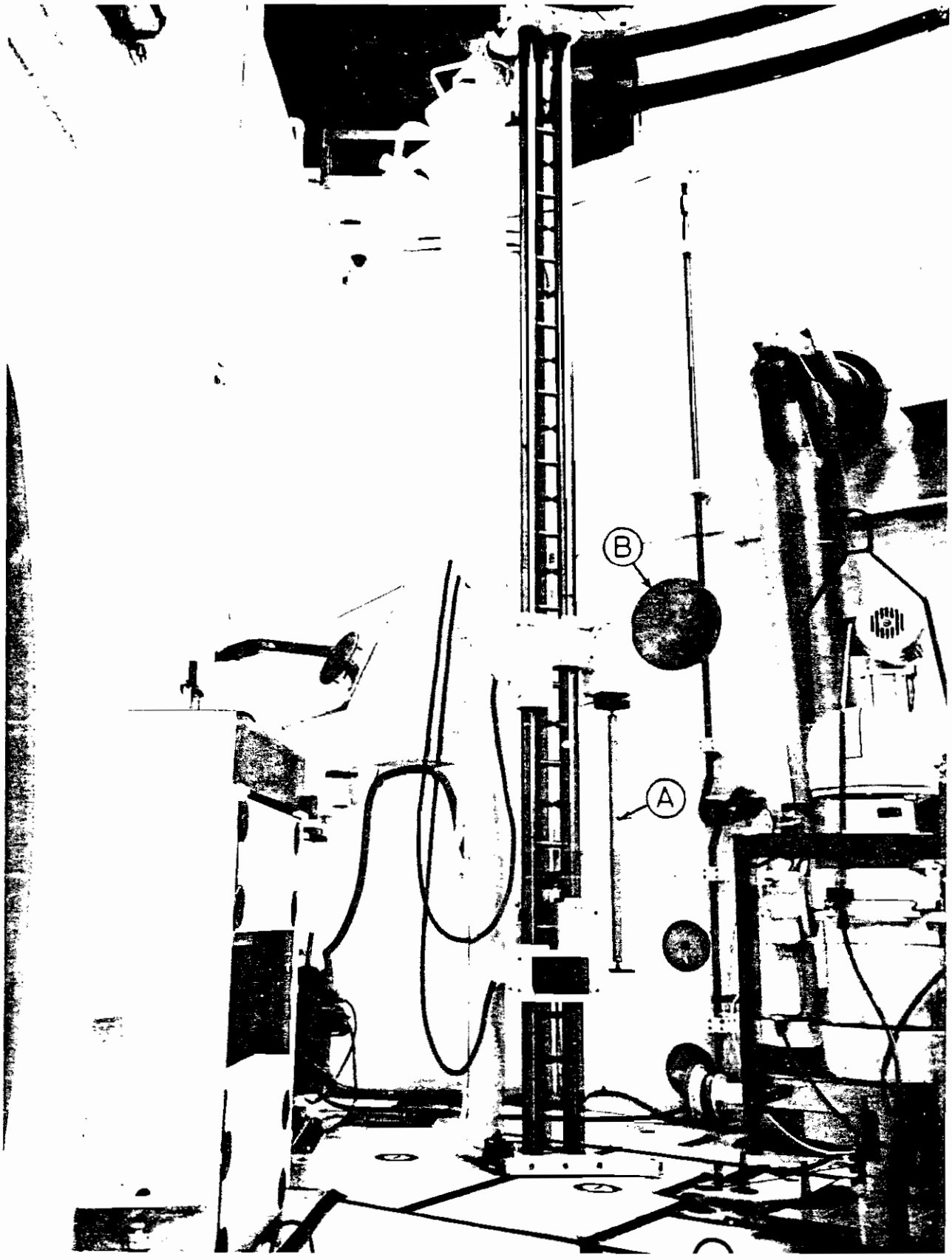

Fig. 17 - Gamma scanning equipment.
A. Fuel rod
B. Collimator

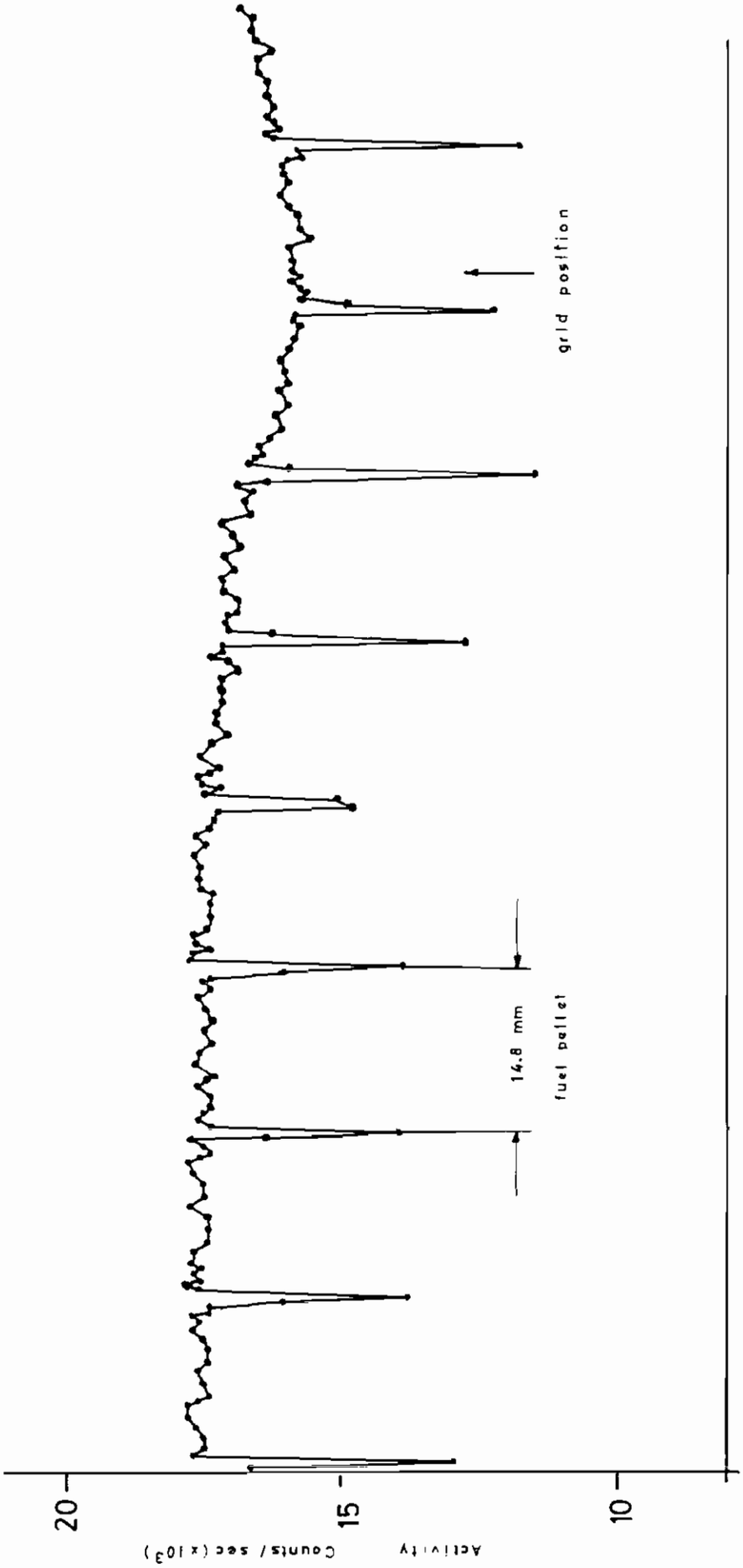

FIG. 18 - Total gamma-activity, part of rod N° 1

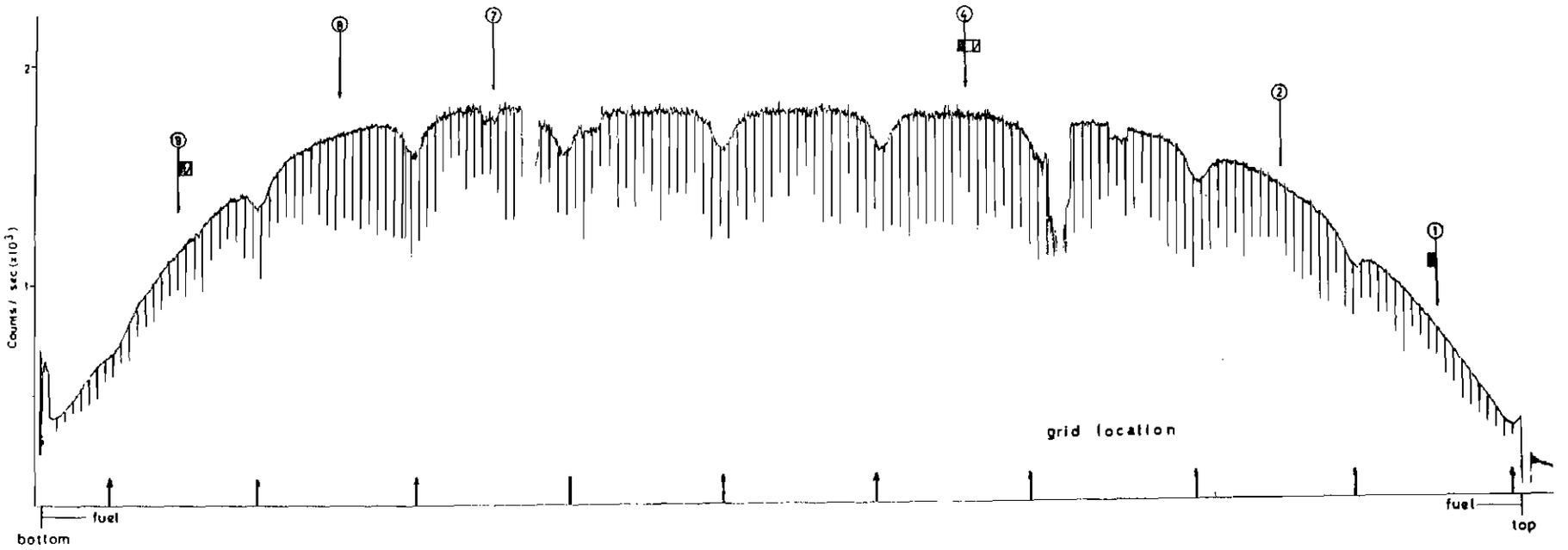

FIG. 19 - Total gamma activity rod No. 1.

▮ Sample for destructive analysis, Ispra.

▯ " " " " , Karlsruhe.

○ Position of gamma spectrometric measurements.

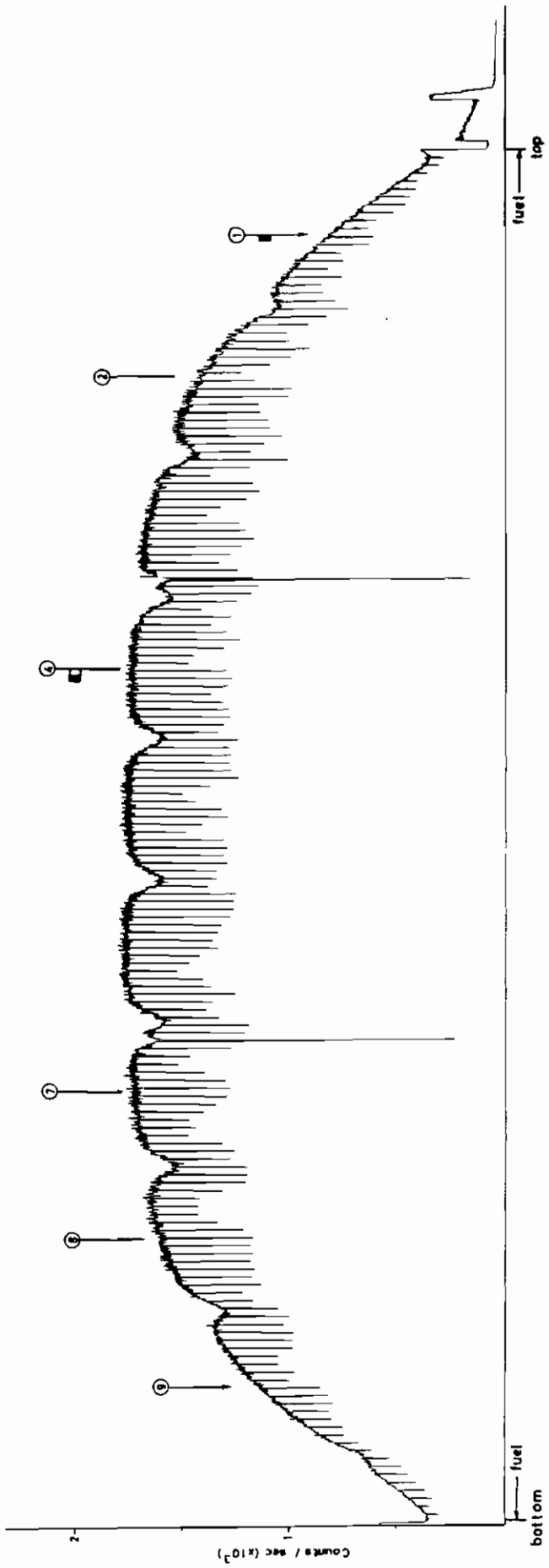

FIG. 20 - Total gamma activity rod No. 2.

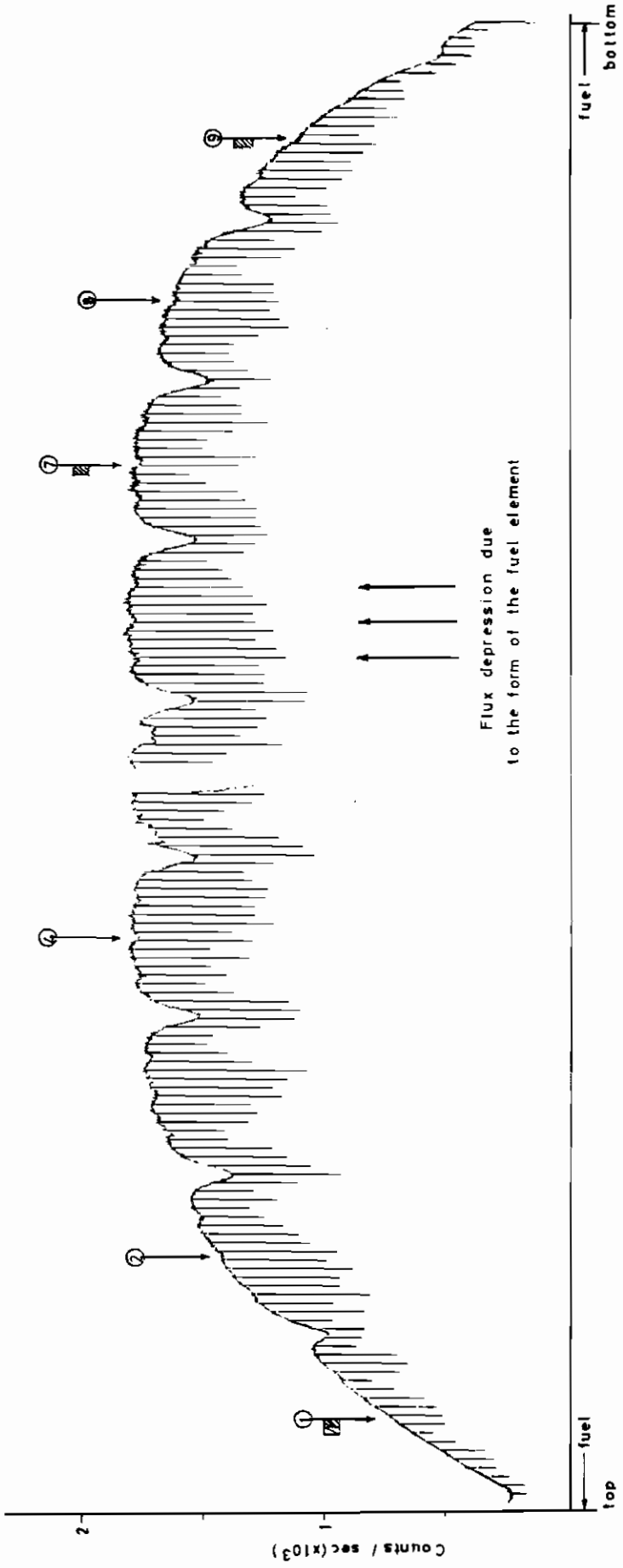

FIG. 21 - Total gamma activity rod No. 3.

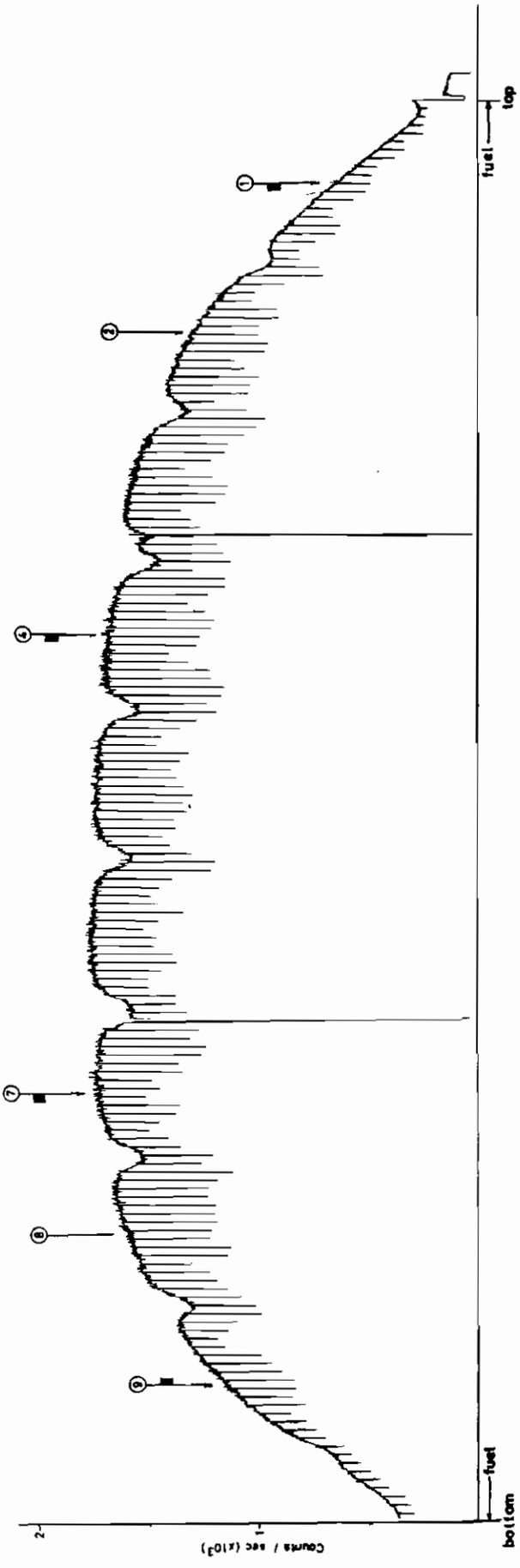

FIG. 22 - Total gamma activity rod No. 4.

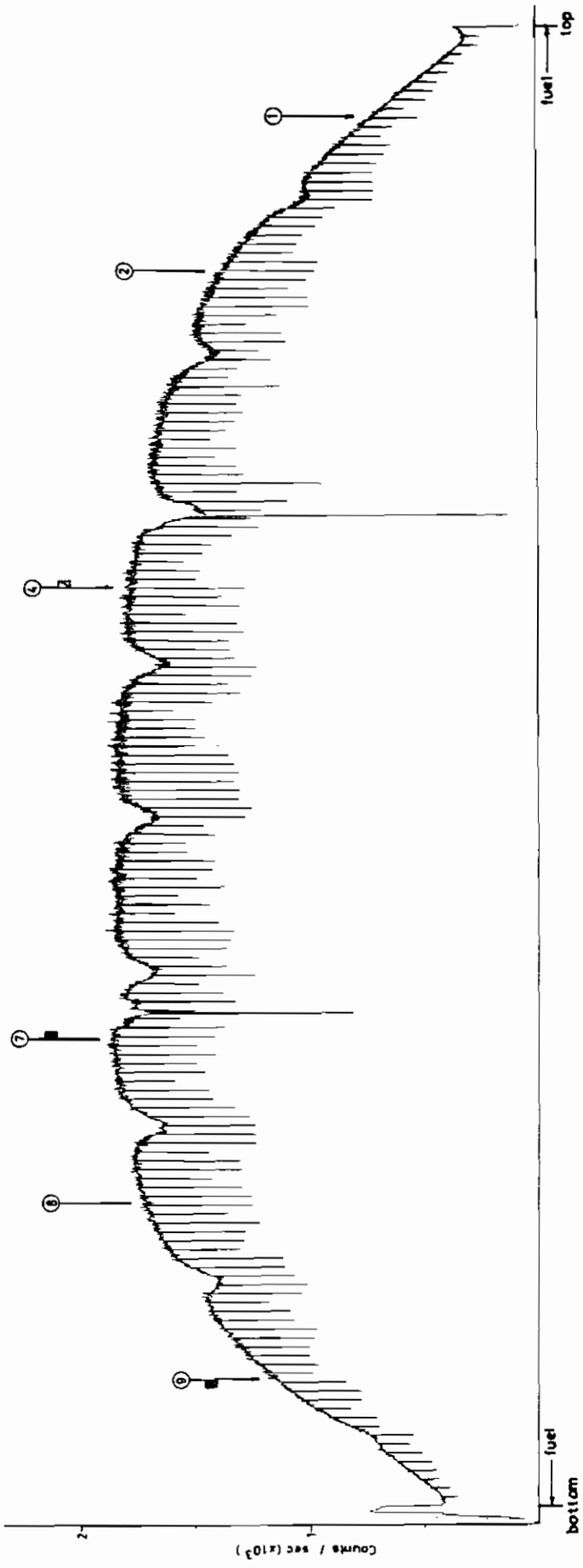

FIG. 23 - Total gamma activity rod No. 5.

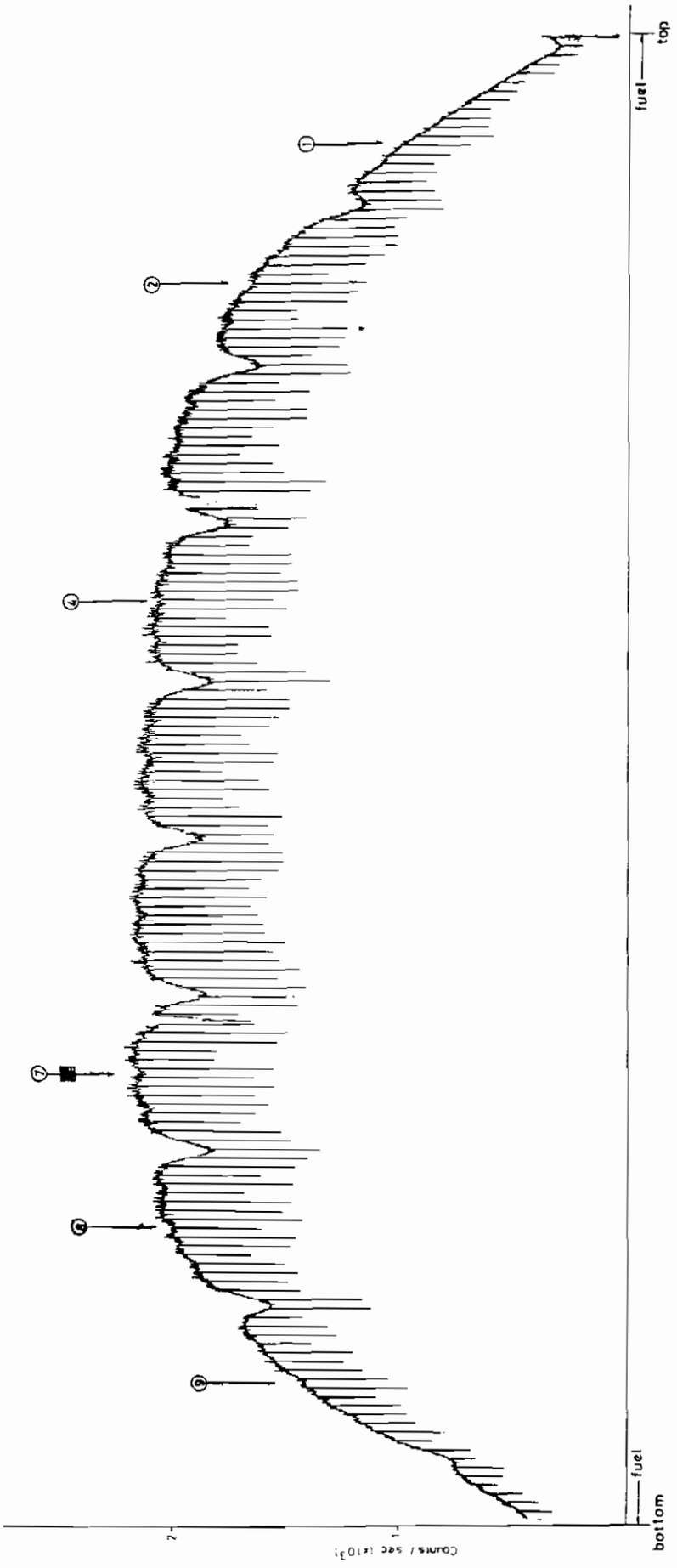

FIG. 24 - Total gamma activity rod No. 6.

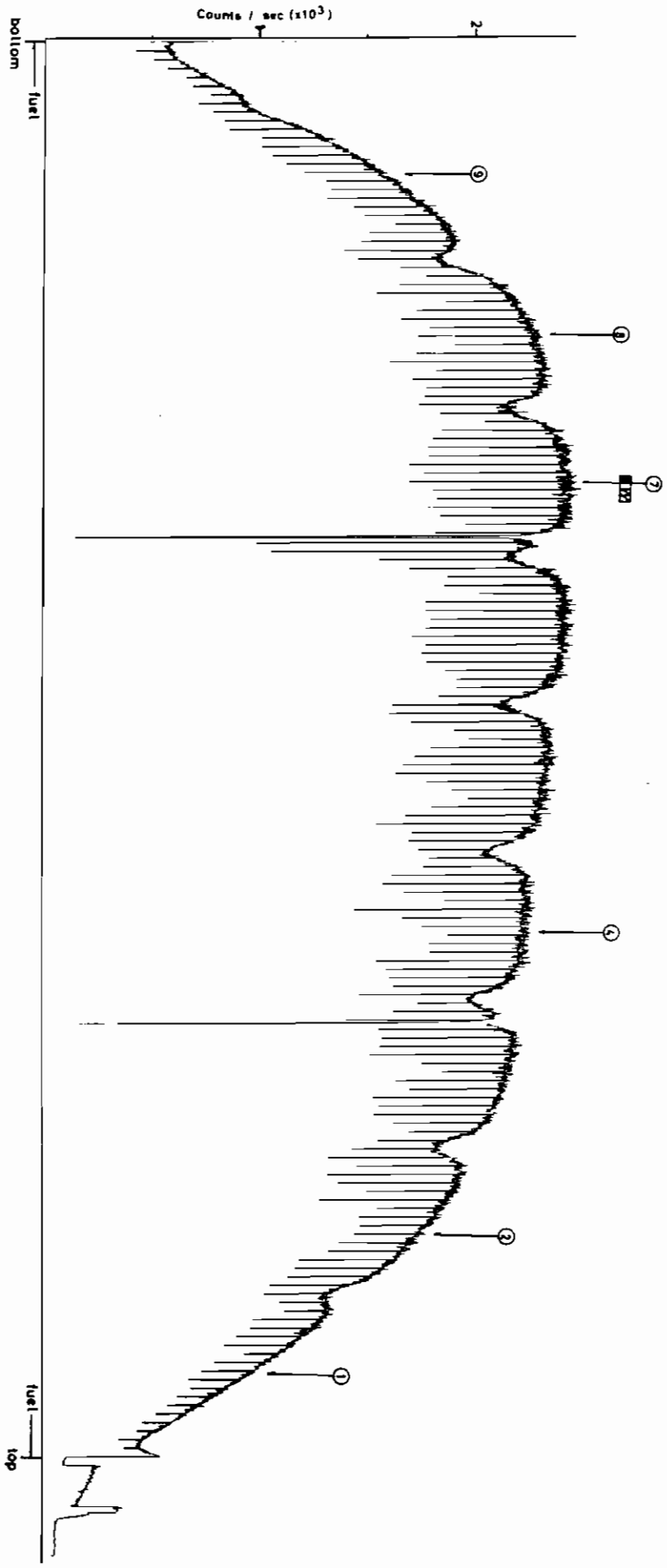

FIG. 25 - Total gamma activity rod No. 7.

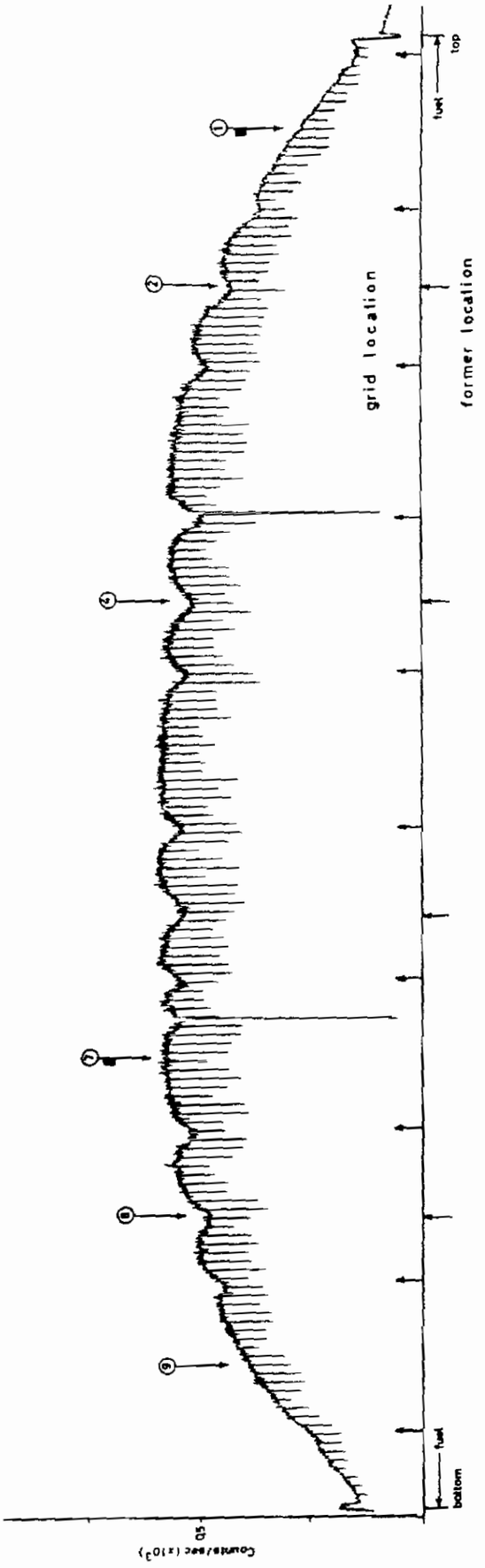

FIG. 26 - Total gamma activity rod No. 8.

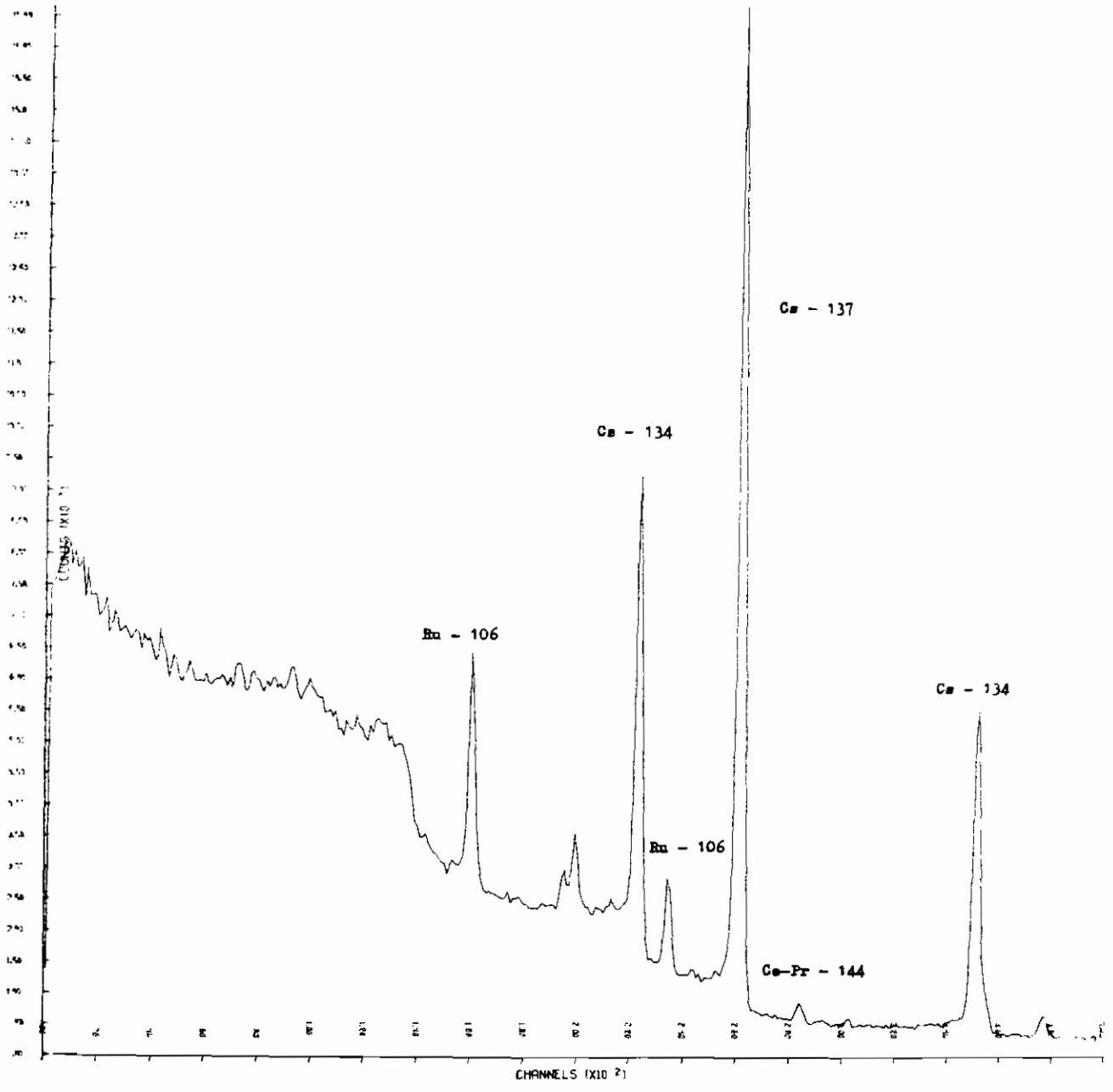

FIG. 27 - Gamma spectrum of fission products from a fuel rod.

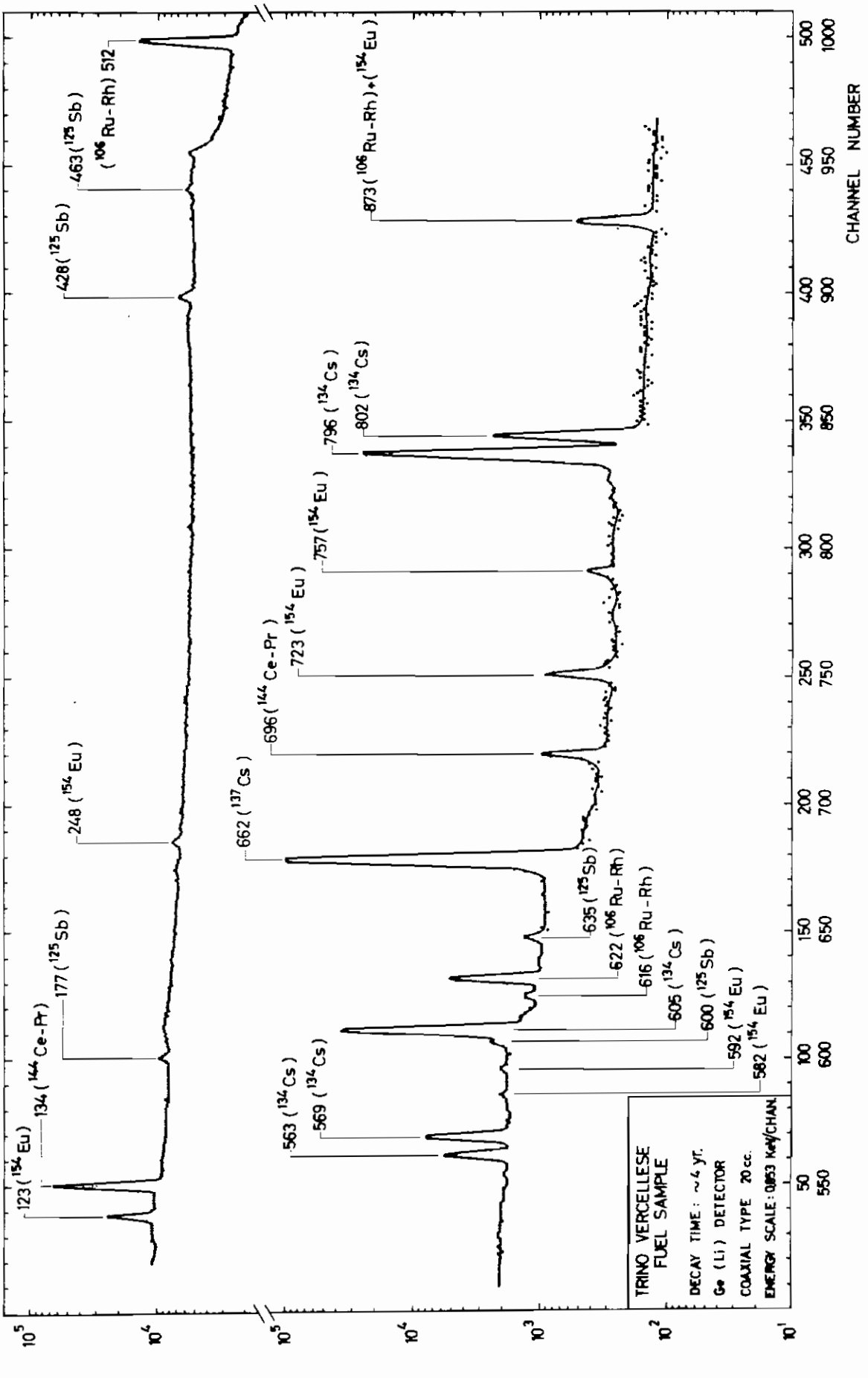

FIG. 28 - Gamma spectrum of fission products from a dissolved fuel sample.

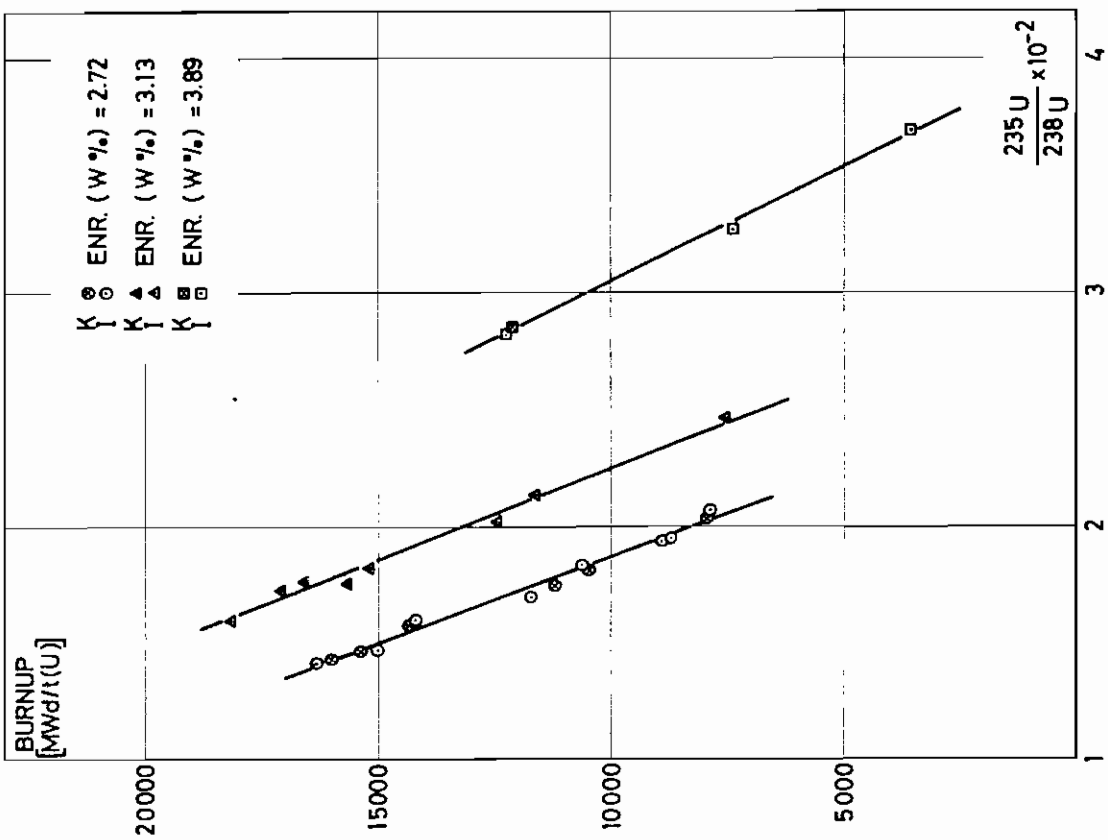

FIG. 29 - Correlation between burnup and U-235 / U-238.

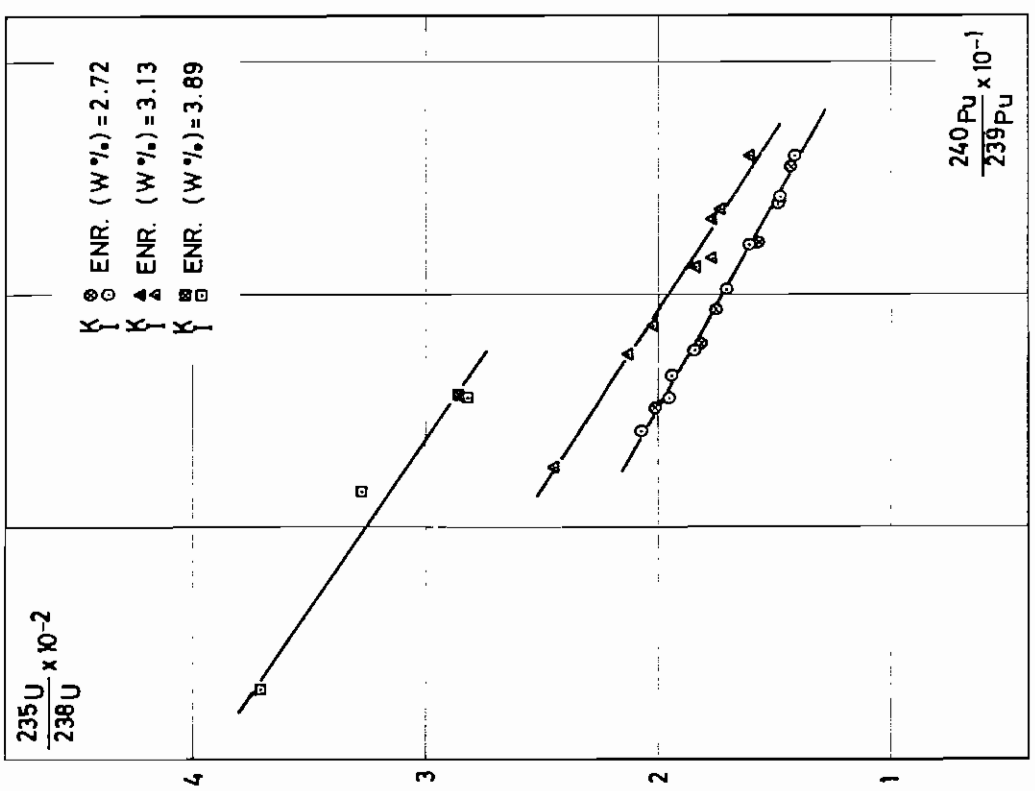

FIG. 30 - Correlation between U-235/U-238 and Pu-240/Pu-239.

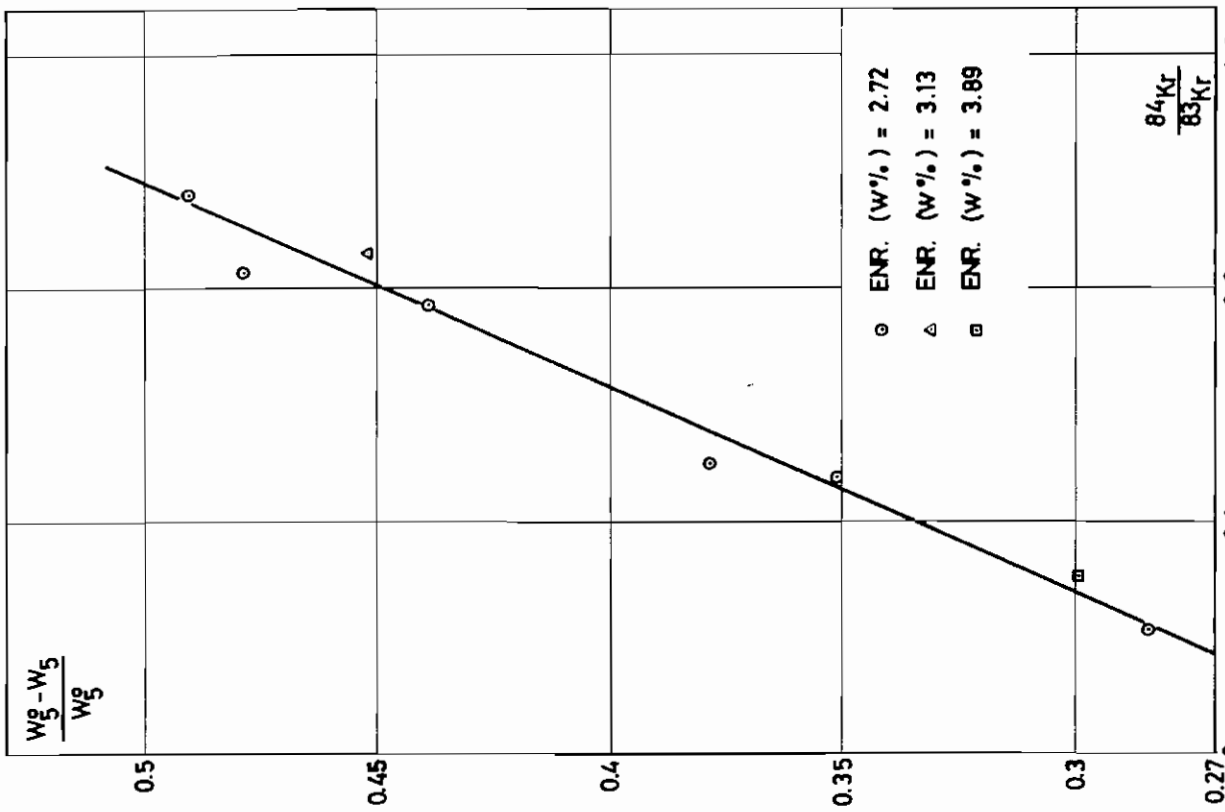

FIG. 31 - Correlation between uranium depletion and Kr-84/Kr-83.

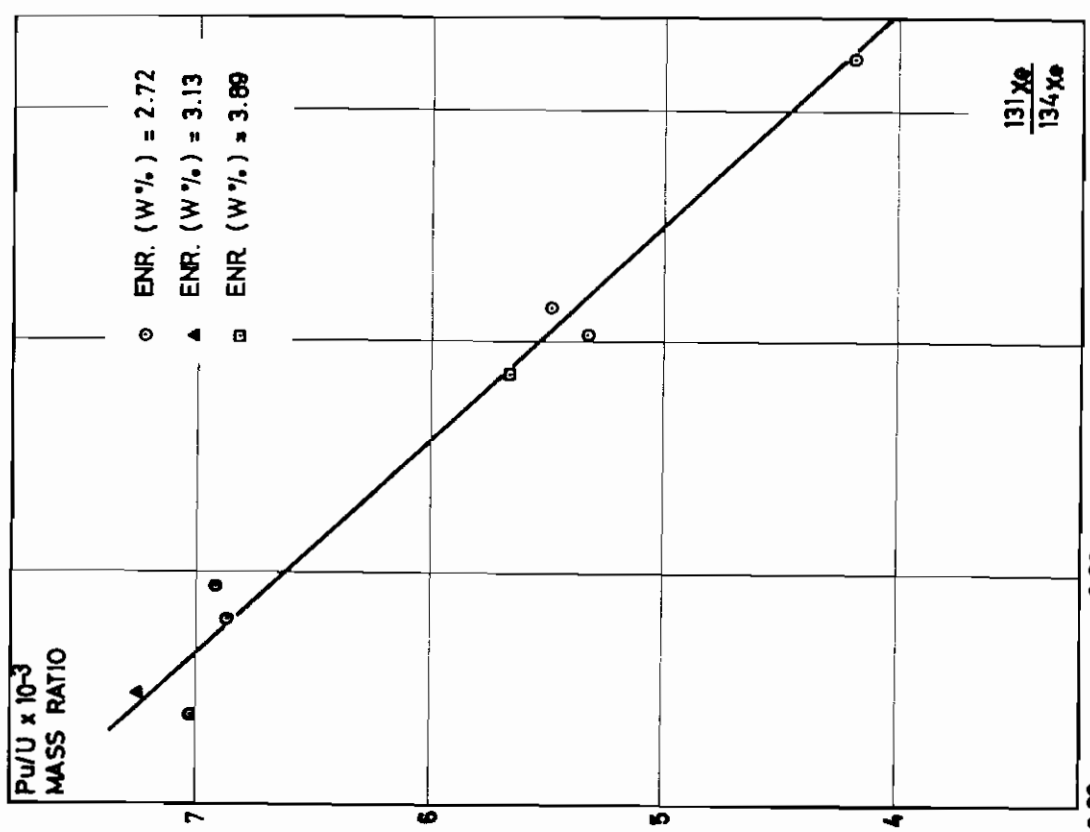

FIG. 32 - Correlation between Pu/U and Xe-131 / XE-134.

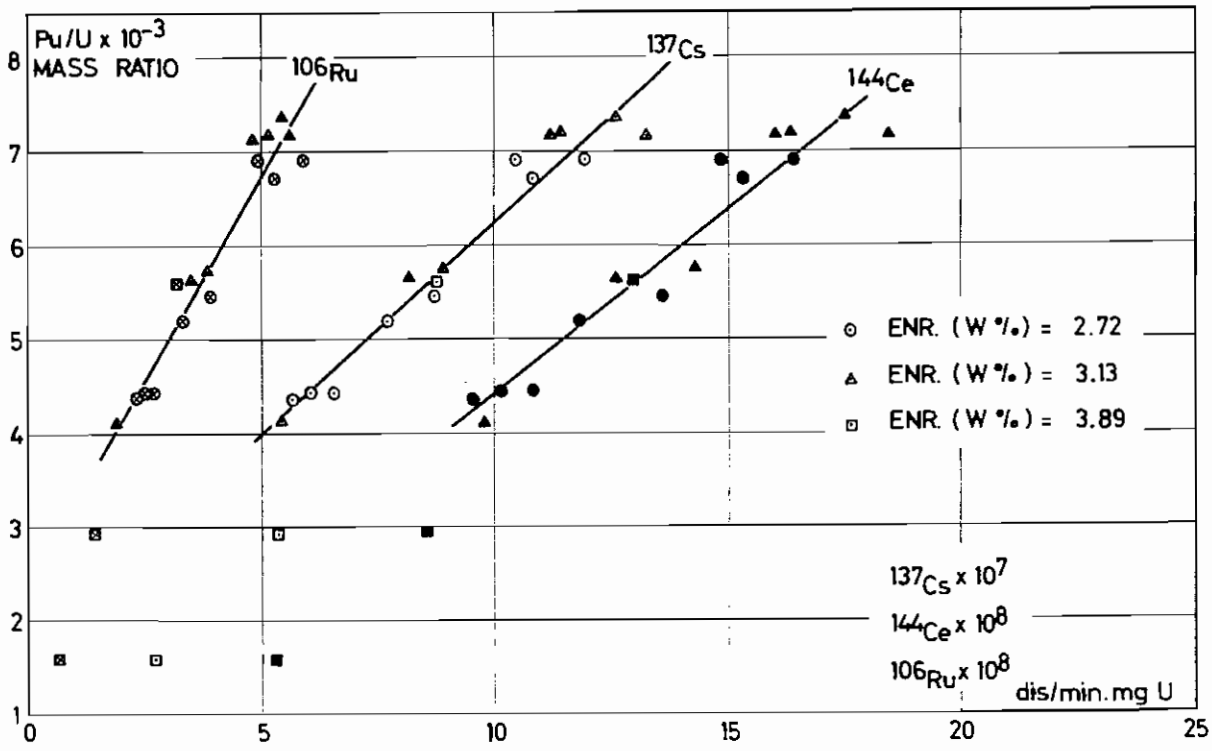

FIG. 33 - Correlation between Pu/U and Cs-137, Ce-144, Ru-106 specific activities.

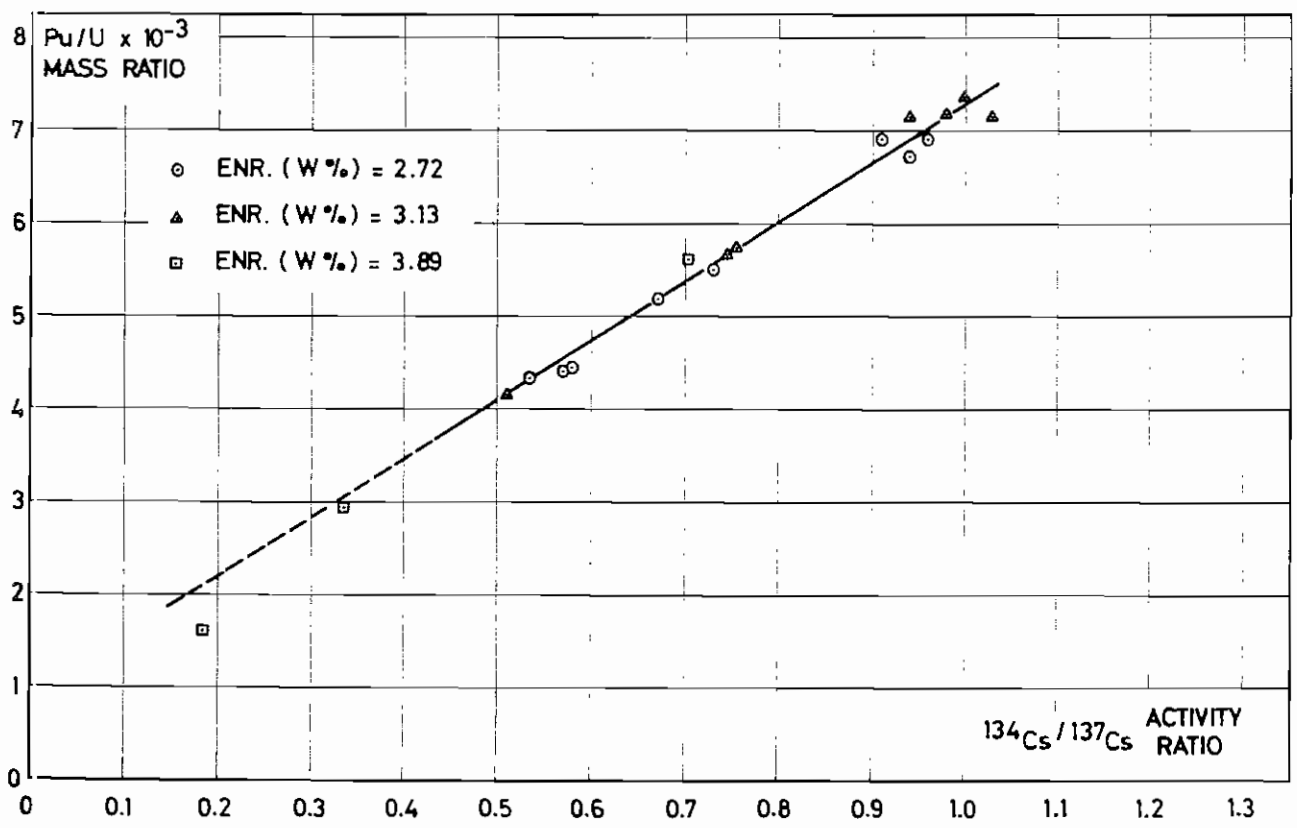

FIG. 34 - Correlation between Pu/U and Cs-134/Cs-137 activity ratio.

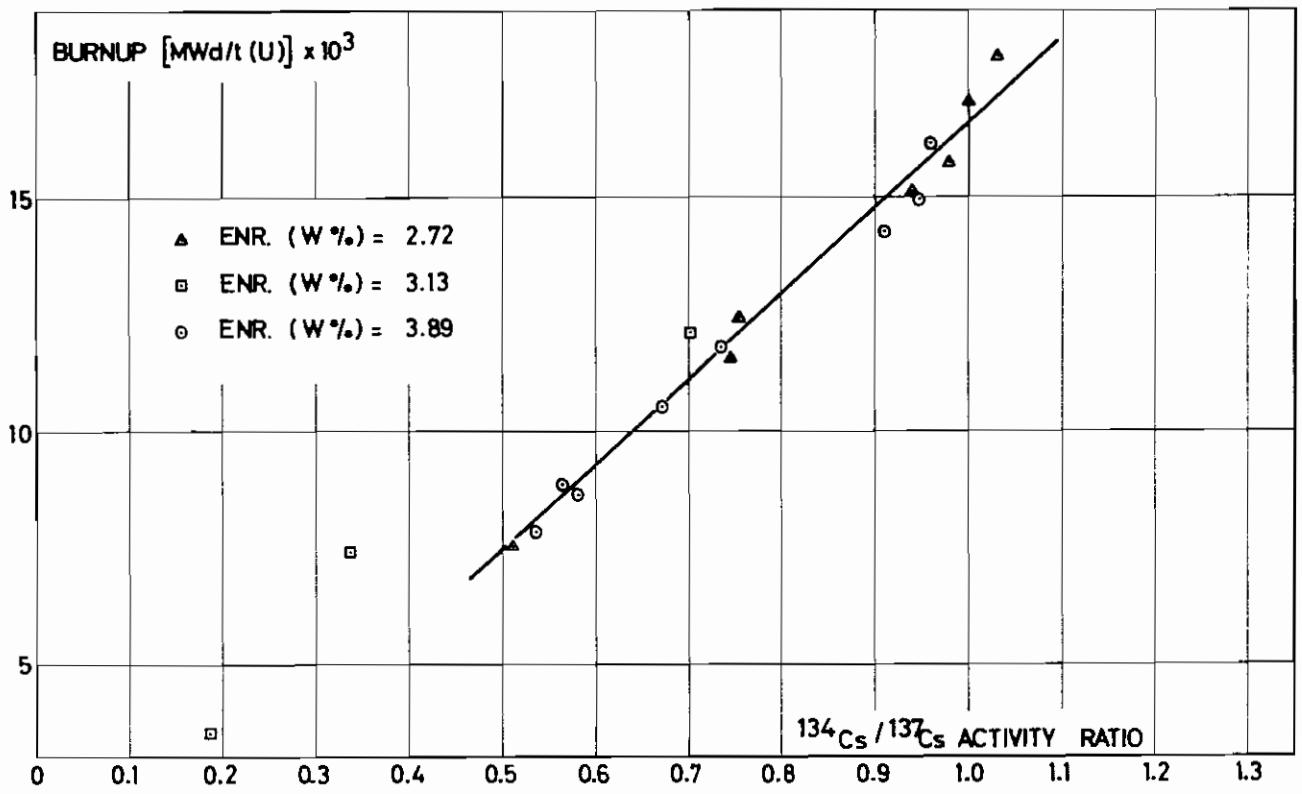

FIG. 35 - Correlation between burnup and Cs-134/Cs-137 activity ratio.

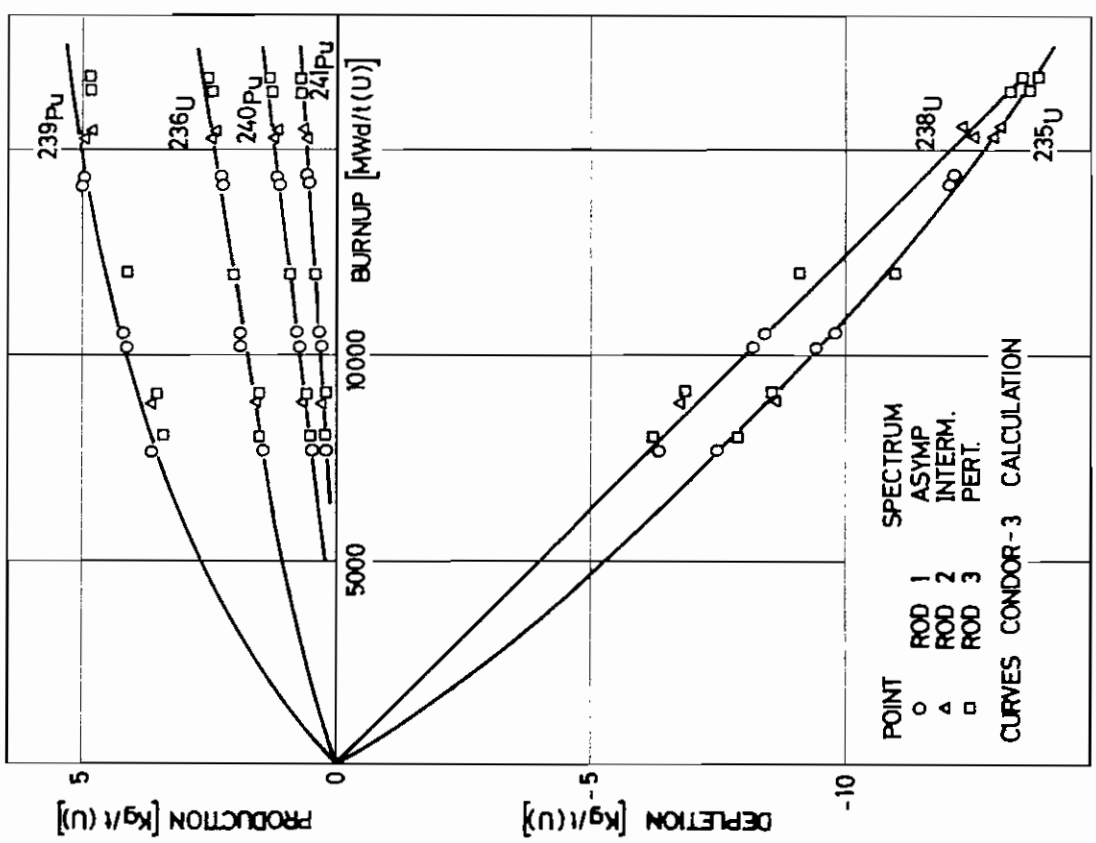

FIG. 36 - Isotopic production and depletion vs. burnup for the inner core region.

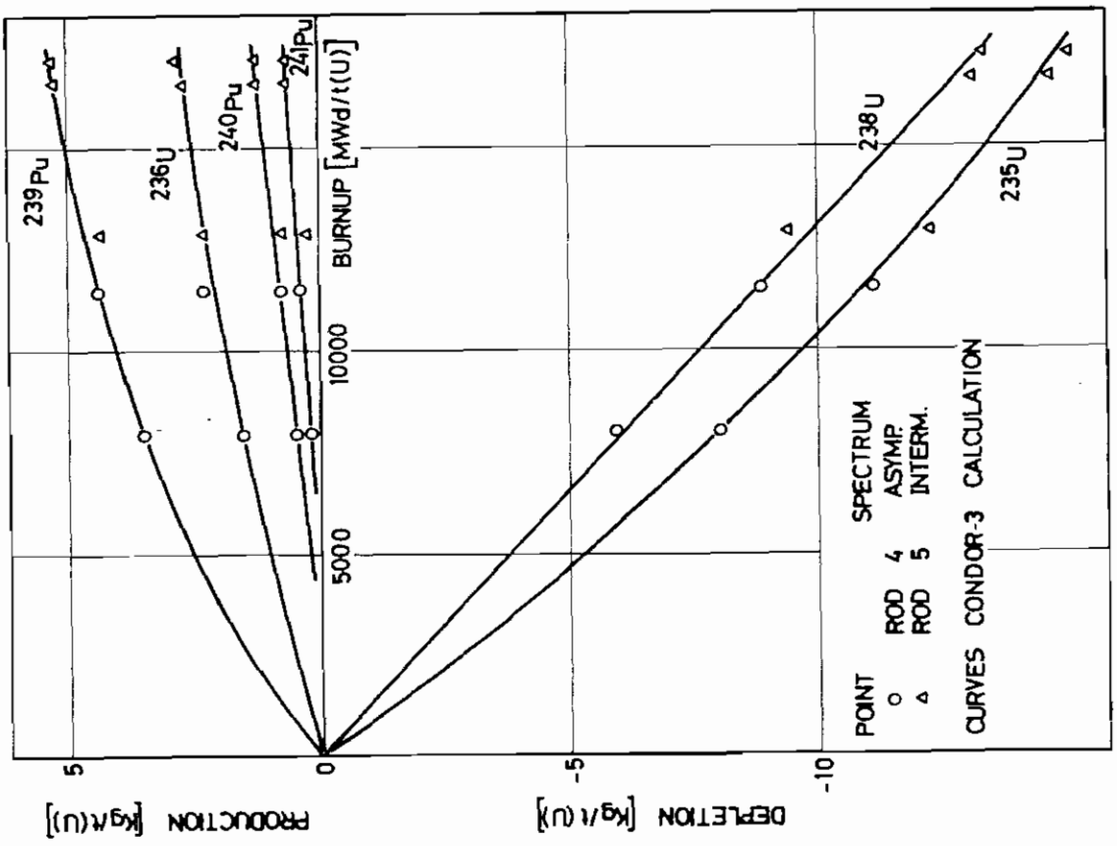

FIG. 37 - Isotopic production and depletion vs. burnup for the intermediate core region.

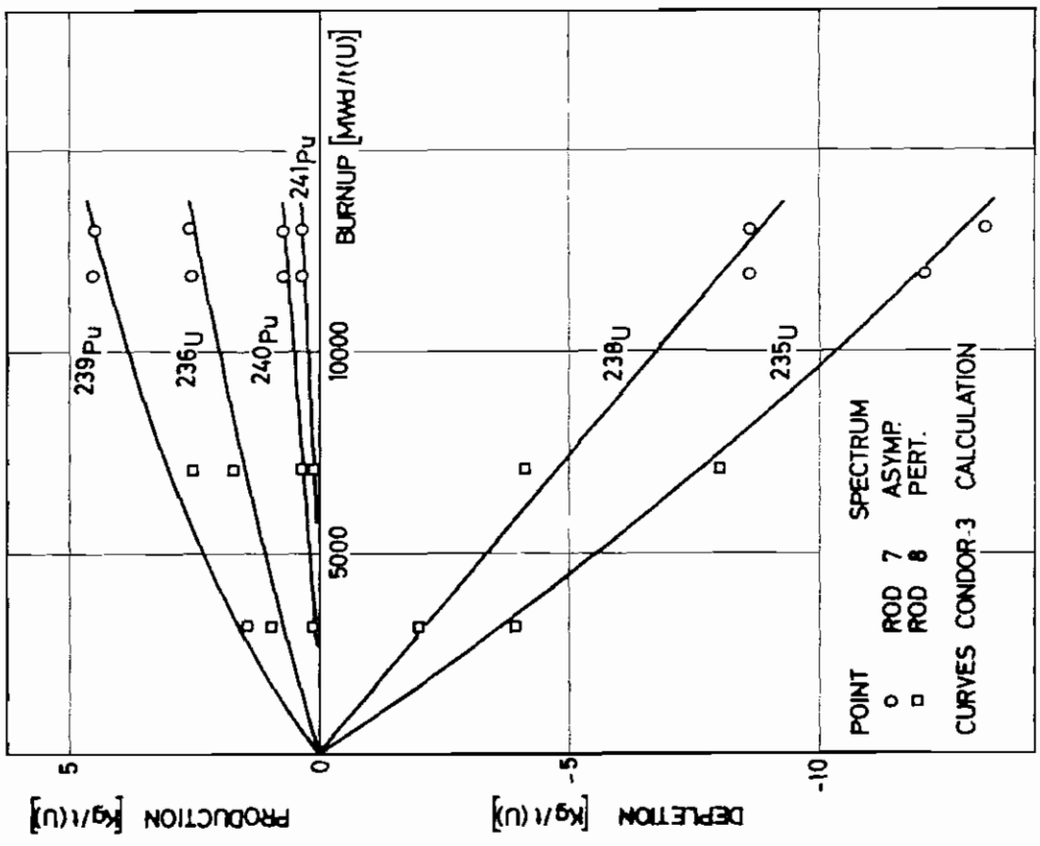

FIG. 38 - Isotopic production and depletion vs. burnup for the outer core region.